The Stellar Populations in the Central Parsecs of Galactic Bulges

Marc Sarzi[2], Hans-Walter Rix[3], Joseph C. Shields[4], Luis C. Ho[5], Aaron J. Barth[6], Gregory Rudnick[7], Alexei V. Filippenko[8], and Wallace L. W. Sargent[9]

ABSTRACT

We present *Hubble Space Telescope* blue spectra at intermediate spectral resolution for the nuclei of 23 nearby disk galaxies. These objects were selected to have nebular emission in their nuclei, and span a range of emission-line classifications as well as Hubble types. In this paper we focus on the stellar population as revealed by the continuum spectral energy distribution measured within the central $0\farcs13$ ($\sim$ 8 pc) of these galaxies. The data were modeled with linear combinations of single-age stellar population synthesis models. The large majority ($\sim 80\%$) of the surveyed nuclei have spectra whose features are consistent with a predominantly old ($\gtrsim 5\times10^9$ yr) stellar population. Approximately 25% of these nuclei show evidence of a component with age younger than 1 Gyr, with the incidence of these stars related to the nebular classification. Successful model fits imply an average reddening corresponding to $A_V \approx 0.4$ mag and a stellar metallicity of (1–2.5)$Z_\odot$. We discuss the implications of these results for

[1]Based on observations obtained with the *Hubble Space Telescope*, which is operated by AURA, Inc., under NASA contract NAS5-26555.

[2]University of Oxford, Astrophysics, Keble Road, OX13RH Oxford, United Kingdom; sarzi@astro.ox.ac.uk

[3]Max-Planck-Institut für Astronomie, Königstuhl 17, D-69117 Heidelberg, Germany; rix@mpia-hd.mpg.de

[4]Physics & Astronomy Department, Ohio University, Athens, OH 45701; shields@phy.ohiou.edu

[5]The Observatories of the Carnegie Institution of Washington, 813 Santa Barbara St., Pasadena, CA 91101-1292; lho@ociw.edu

[6]Department of Physics & Astronomy, 4129 Frederick Reines Hall, University of California, Irvine, CA 92697-4575; barth@uci.edu

[7]Max-Planck-Institut für Astrophysik, Karl-Schwarzschild-Strasse 1, D-85741 Garching, Germany; grudnick@mpa-garching.mpg.de

[8]Department of Astronomy, University of California, Berkeley, CA 94720-3411; alex@astro.berkeley.edu

[9]Astronomy Department, California Institute of Technology, MS 105-24, Pasadena, CA 91125; wws@astro.caltech.edu

the understanding of the star formation history in the environment of quiescent and active supermassive black holes. Our findings reinforce the picture wherein Seyfert nuclei and the majority of low-ionization nuclear emission-line regions (LINERs) are predominantly accretion-powered, and suggest that much of the central star formation in H II nuclei is actually circumnuclear.

Subject headings: galaxies: bulges — galaxies: nuclei — galaxies: stellar content

1. Introduction

The centers of galaxies hold special interest as the locations of unusual energetic phenomena. It is now commonly accepted that most galaxies harbor central supermassive black holes (SMBHs) that in the past may have shone as powerful active galactic nuclei (AGNs). The fueling of luminous AGNs requires substantial gas concentrations that might also be favorable sites for star formation, and the formation of a dense star cluster is in fact one means of spawning a SMBH (e.g., Rees 1984). In the present Universe, many galactic nuclei exhibit emission-line activity at low levels that apparently derives from a variable mix of accretion power and star formation (e.g., Ho, Filippenko, & Sargent 1997). Emission-line ratios provide a basis for classifying objects into standard categories that, to varying degrees of confidence, are identified with specific power sources. While classification as a Seyfert or H II nucleus is routinely associated with nonstellar accretion and O stars as dominant energy sources, respectively, many galaxies are classified as low-ionization nuclear emission-line regions (Heckman 1980, LINERs) or LINER/H II "transition nuclei" (e.g., Filippenko & Terlevich 1992; Ho, Filippenko, & Sargent 1993) which are more ambiguous in their interpretation. Evidence increasingly suggests that LINERs are primarily accretion-powered (e.g., Ho, Filippenko, & Sargent 2003; Filippenko 2003), but the situation is less clear for the transition sources.

The direct detection of young stellar populations in galactic nuclei is an important means of quantifying star formation in these environments and possible connections to emission-line activity. Nearby examples suggest that recent star formation is not unusual. The Milky Way, IC 342, and NGC 4449 all have central young stellar clusters (Krabbe et al. 1995; Böker et al. 2001; Böker, van der Marel, & Vacca 1999), and our neighbors M33 and M31 also have blue nuclei that are most likely consistent with the presence of young stars (Lauer et al. 1998). Moreover, imaging surveys with the *Hubble Space Telescope* (*HST*) have shown that a compact star cluster is often present in the center of spiral galaxies (Phillips et al. 1996; Carollo, Stiavelli, & Mack 1998; Matthews et al. 1999), in particular in the latest Hubble types (Böker et al. 2002). If proved young, such clusters may help account for the high

frequency (41%) of H II nuclei in nearby galaxies (Ho, Filippenko, & Sargent 1997), and may also have bearing on transition nuclei.

Most existing studies of stellar populations and nebular emission in galaxy centers have been carried out from the ground, and in probing "nuclei" are thus limited to studying regions that may actually be several hundreds of parsecs in scale. Considerable structure may exist on smaller scales, and the spatial distribution of star formation within such a region is of particular interest. A number of ultraviolet (UV) *HST* surveys have shown that star formation in galactic nuclei often takes place in circumnuclear rings (e.g., Maoz et al. 1996). If all bulges harbor a SMBH, there are reasons to believe that it may be difficult to form stars in their very central regions. In particular, the tidal field induced by a SMBH may suffice to disrupt molecular clouds before they can gravitationally collapse. Observationally, however, a number of studies have shown that SMBHs and young stellar clusters can coexist on very small scales, at least in some Seyfert 2 and LINER nuclei (Heckman et al. 1997; González-Delgado et al. 1998; Colina et al. 2002) and in the Milky Way (e.g., Genzel et al. 2003).

Probing galaxy centers with the highest possible spatial resolution is thus of great value for understanding what powers "nuclear" activity, and how star formation proceeds in these zones. The recent *HST* surveys of Peletier et al. (1999) and Carollo et al. (2001, 2002) represent excellent examples of how high-resolution images have already helped in making steps in this direction. The observed visual to near-infrared colors indicate that the vast majority of disk galaxy centers are very red, consistent with intermediate to very old stellar populations that are substantially obscured by interstellar material. Yet, with only broad-band colors it is difficult to disentangle the effects of an old stellar population from those of reddening by dust, super-solar metallicity, or an active nucleus.

For this reason we undertook a survey of nearby nuclei with the Space Telescope Imaging Spectrograph (STIS) on board *HST* (the SUNNS survey), acquiring moderate-resolution blue and red spectra for 23 galaxies to study both their nuclear stellar populations and emission-line kinematics, and to detect in particular the presence of very young stars or SMBHs. In this paper we present a study of the nuclear stellar populations of the SUNNS sample galaxies, based on the fitting of synthetic stellar population models to the observed blue spectra. After we submitted this paper for publication, we learned of related work by González-Delgado et al. (2004) which reaches broadly similar conclusions.

The paper is organized as follows. In §2 we show the nuclear spectra for our sample objects, in §3 we describe our analysis method, and in §4 we present our results. Our analysis includes models based on single-age stellar populations (§4.1) or with extended star formation histories (§4.2) and addresses the effect of super-solar metallicities (§4.3). From

the model fitting we derive conservative upper limits on the presence of very young stars and constraints on the need for absorption-line dilution by a featureless continuum (§4.4). We discuss these results in §5 and draw our conclusions in §6.

2. Observations and Data Reduction

The nuclear spectral energy distributions (SEDs) modelled in this paper have been extracted from the two-dimensional (2-D) *HST*-STIS spectra acquired in the course of the SUNNS spectroscopic survey of 23 galactic nuclei (Shields et al. 2004b). The SUNNS targets were drawn from the Palomar spectroscopic survey of nearby galaxies (Filippenko & Sargent 1985; Ho, Filippenko, & Sargent 1997) and include all galaxies within 17 Mpc known to have optical Hα or [N II] λ6583 line emission ($\gtrsim 10^{15}$ ergs s^{-1} cm^{-2}) within a $2'' \times 4''$ aperture. The sample was also chosen to investigate the nature of nuclear activity and includes Seyfert galaxies, LINERs, LINER/H II transition objects, and H II nuclei. Basic parameters of the sample galaxies are given in Table 1.

Spectra were acquired with the STIS $0\farcs2 \times 50''$ slit, and 5-pixel-wide ($\sim 0\farcs25$) extractions were used to generate one-dimensional (1-D) spectra of the nuclei. The resulting aperture of $0\farcs2 \times 0\farcs25$ is equivalent in area to a circular aperture with radius $r = 0\farcs13$, corresponding to 8.2 pc for the mean sample distance of ~ 13 Mpc. The G430L and G750M gratings were employed to obtain spectral coverage of 3000–5700 Å and 6300–6850 Å, respectively. In the present analysis we utilize only the G430L spectra, since these data cover spectral features providing the strongest constraints on the stellar population. As extinction by interstellar dust will be an important factor in our modelling, we have corrected the observed fluxes for Galactic foreground reddening, using A_V values from Schlegel, Finkbeiner, & Davis (1998) and the Cardelli, Clayton, & Mathis (1989) extinction law with $R_V = 3.1$. The full-width at half maximum (FWHM) resolution for the G430L spectra is 7.8 Å for extended sources. Full details concerning the observations are presented by Shields et al. (2004b).

The final extracted and dereddened nuclear G430L spectra, along with their associated errors, are shown for all our sample galaxies in Figure 1. Their heterogeneity is clear, in terms of both their quality and the kind of spectral energy distribution they are sampling. The signal-to-noise ratio (SNR) per pixel is ∼2–15 and ∼15–50 at the blue and red ends, respectively. Most nuclear spectra have a strong 4000 Å break, as well as Mg and Fe absorption features (around 5175 Å and 5270 Å, respectively), indicative of old stellar populations (e.g., NGC 3992, NGC 4459, or NGC 4596), but some show strong Balmer absorption lines underscoring the presence of younger components (e.g., NGC 3368 and NGC 3489). Many nuclei display obvious nebular emission, which must be excluded when analyzing the under-

lying stellar spectrum. Contamination by line emission is particularly strong for the Seyfert galaxy NGC 3982 and the two LINERs NGC 4203 and NGC 4450, where a very broad pedestal of Balmer emission has already been reported by Shields et al. (2000) and Ho et al. (2000), respectively. Figure 1 shows for each galaxy the spectral regions omitted for this reason in our analysis.

2.1. Bulge-Light Contamination

An important issue is the extent to which our projected nuclear spectra sample the actual nuclear regions of our galaxies. To address this matter, we derived for each object an estimate for the intrinsic luminosity density profile, which can be used to determine the ratio between the light emitted within the central sphere of radius equal to our central aperture, $r \approx 0\farcs13$, and the light collected along the line of sight in a cylindrical beam with the same radius. The luminosity density profile was estimated by assuming spherical symmetry and deprojecting the stellar surface brightness distribution in the STIS acquisition image. The multi-Gaussian algorithm adopted for this purpose by Sarzi et al. (2001) was applied to circularly averaged surface brightness profiles extracted using the IRAF[1] task ELLIPSE. Dust absorption causes problems for this approach in some cases, but the analysis overall indicates that typically ∼60% of the flux collected within our central aperture should come from regions within ~ 8 pc of the center.

As our sample consists of relatively early-type disk galaxies (S0 to Sb) with intermediate inclinations (average inclination angle 44°, Table 1), contamination of our spectra by extranuclear stars seen in projection is presumably due mostly to bulge stars, rather than stars in the galactic disk.

3. Analysis Method

To interpret our nuclear spectra, we fit them with synthetic population models that are based on a variety of star formation histories, metallicities, and reddenings. To simulate extended star formation histories, we used linear combinations of single-age stellar population synthesis templates to fit the nuclear spectra directly in pixel space, following Rix et al.

[1]IRAF is distributed by the National Optical Astronomy Observatories, which are operated by the Association of Universities for Research in Astronomy, Inc., under cooperative agreement with the National Science Foundation.

(1995). This algorithm derives simultaneously the optimal combination of template spectra and the kinematical broadening required to match the data. To establish the relative weight of different model SEDs in explaining each galaxy nuclear spectrum, we proceeded through the following steps.

1. Select one template from the set of model SEDs and use it to obtain an initial estimate for the line-of-sight velocity distribution (LOSVD), which here in practice consists of a simple Gaussian.

2. Use the LOSVD obtained in step (1) to shift and broaden *all* of the model SEDs, and find the linear combination that best matches the observed spectrum, using a non-negative least-squares algorithm. This prescription assumes that different stellar populations in a given nucleus share the same kinematics.

3. Use the linear combination of weights obtained in step (2) and the original model SEDs to construct an unbroadened optimal template, which is appropriate for matching the strength of spectral features in the observed spectrum.

4. Repeat steps (1), (2), and (3) using this first optimal template in order to derive an improved LOSVD, model SED weights, and optimal template.

By working in pixel space rather than Fourier space, it is straightforward in steps (2) and (3) to exclude wavelength intervals that are contaminated by emission lines. Inspection of the fit residuals enable a better location of such features.

Our library of template spectra is based on the Bruzual & Charlot (2003, hereafter B&C) model SEDs for single-age stellar populations with a Salpeter (1955) initial mass function, with 11 different ages T_i spanning 1 Myr to 10 Gyr. The specific ages employed are $\log T_i = 6.0, 6.5, 7.0, 7.5, 8.0, 8.5, 9.0, 9.25, 9.50, 9.75,$ and 10.0, where T_i is expressed in years. In our analysis we use exclusively B&C model SEDs with solar and 2.5 times solar metallicity. These models have spectral resolution (FWHM = 3 Å) higher than that of our observations, and thus are well suited for obtaining detailed information from spectral features in the data. Figure 2 shows the single-starburst population (SSP) models adopted for our analysis.

In our fit analysis, we included the possibility of interstellar reddening intrinsic to the source, which we modeled using sets of B&C templates modified by different A_V values and the Cardelli, Clayton, & Mathis (1989) extinction law. We considered fractions of absorbed flux at 5512 Å amounting to 9, 17, 24, 30, 37, 42, 48, 52, 56, and 60%, corresponding to A_V of 0.1, 0.2, 0.3, 0.4, 0.5, 0.6, 0.7, 0.8, 0.9, and 1.0 mag, respectively.

Since the B&C model SEDs correspond to "clusters" of 1 $M_\odot$, both in stars and the gaseous material ejected by them during their evolution, the linear fit coefficients are total mass weights m_i. The corresponding stellar mass weights are $m_i^\star = f_i^\star m_i$, where $f_i^\star$ is the age-dependent fraction of the total mass which is in stars. The stellar mass-weighted mean age is then given by $\overline{T}_{mass} = (\sum_i T_i m_i^\star)/\sum_i m_i^\star$ for the best multi-age models. Alternatively, if template SEDs are scaled to the same luminosity, the relative weights l_i reflect the luminosity-weighted mean age $\overline{T}_{light} = (\sum_i T_i s l_i)/\sum_i l_i$. Scaling all the 1-$M_\odot$ model SEDs to the same luminosity is equivalent to dividing them by their total mass-to-light ratio Υ times a constant, so that the light weights are just $l_i \propto m_i/\Upsilon_i = m_i^\star/\Upsilon_i^\star$, where $\Upsilon^\star = \Upsilon f_i^\star$ is the stellar mass-to-light ratio. It follows that $\overline{T}_{light}$ is always smaller than $\overline{T}_{mass}$ because older SSP models always have larger mass-to-light ratios than younger ones. Unless the observed SED is clearly dominated by old stars, the luminosity-weighted mean age estimate $\overline{T}_{light}$ is more robust than $\overline{T}_{mass}$, because any small error in matching the observed fluxes becomes more relevant for older stars than for younger stars when it comes to addressing mass fractions. On the other hand, in the limit of a small component of young stars intermingled with an old population, a varying contribution of young stars will shift $\overline{T}_{light}$ much more than $\overline{T}_{mass}$. In this situation we are more likely to obtain an upper limit on the contribution of young stars, and the derived luminosity-weighted mean age $\overline{T}_{light}$ will still represent a safe lower limit for the age of the nuclear population.

In the following analysis we therefore focus on the $\overline{T}_{light}$ values, as robust estimates or lower limits on the stellar population age. Conversely, the mass fractions of young stars ($\lesssim$ 1 Gyr) should be regarded as upper limits. We emphasize that these statements apply to the stellar populations to the extent that they are traced by optical light. Our analysis is not sensitive to young populations subject to large extinction, which in principle could be present but elude detection in our data.

Alternatively, we could have described the stellar populations of our sample nuclei through standard Lick/IDS indices, to be used in diagnostic diagrams (e.g, Worthey 1994; Vazdekis 1999). Given the considerable amount of nebular emission often present in our nuclear spectra, the best choice for an age indicator would have been the Hγ_A index introduced by Worthey & Ottaviani (1997); this feature is less contaminated by gas emission than is Hβ, since the nebular flux decreases rapidly with increasing order for the Balmer lines. Furthermore, since many of our nuclear spectra are fairly noisy, as a metallicity indicator we could have considered the Fe3 index of Kuntschner (2000), which combines three strong iron lines and is also somewhat less sensitive to non-solar metal abundance ratios. However, the limited spectral resolution of our G430L spectra does not allow accurate measurement of stellar velocity dispersions from these data, which thus precludes a corresponding correction of the derived indices. In particular, the kinematical broadening would reduce the line strength of

the metallicity indicator (Kuntschner 2000), which would bias us to infer older ages. As the effect is increasingly important for larger velocity dispersions, this problem would have been particularly serious in the case of our nuclear spectra, because stellar velocity dispersions are expected to reach large values in proximity of the central SMBH. The use of line indices also does not readily allow for the influence of an AGN continuum, which should be considered given indications that many of our sample members have an accretion-powered source. A template superposition approach consequently is the preferred methodology for interpreting the current data.

4. Results

4.1. Single-Starburst Population Models

For an initial description of the nuclear stellar population in our sample galaxies, we determined which of the single-age solar-metallicity model SEDs considered alone best matched the observed spectrum for each source. In our analysis we left the intrinsic A_V as a parameter free to assume any of the values specified in §3. Table 2 lists the ages and A_V values obtained from this fitting exercise, along with the corresponding χ^2 values per degree of freedom (χ^2_ν) as an indication of the quality of each model. Clearly, some spectra are poorly described only by reddened single-age populations. Nevertheless, the most immediate and significant finding is that the populations tend to be old — the single-age values for most reliable models exceed $10^{9.5}$ yr ≈ 3 Gyr. Noticeable exceptions to this trend are NGC 278, NGC 3351, and NGC 3368, for which a relatively young population is able to explain most observed features. On average, the best-fit estimate of internal extinction is modest ($\overline{A}_V = 0.3$ mag), but many of the reddening values are not reliable in light of problems with the quality of the model fit.

4.2. Multiple-Starburst Population Models

4.2.1. Multi-Component Fits

Since it is very probable that the galaxy nuclei contain composite stellar populations, we repeated our analysis with linear combinations of template SEDs drawn from the full set of solar-metallicity SSP models. The intrinsic A_V was again left as a free parameter, with a common reddening assumed for all templates in modeling a given source. This approach generates estimates of the luminosity-weighted mean age and the mass fraction of young stars ($\lesssim$1 Gyr) as described in §3, and provides an indication of whether it is necessary to invoke

multiple or extended star-formation episodes, or very young stars (few Myr), to explain the observed SEDs. If two or more templates representing adjacent steps in our age grid are assigned comparable weights, we typically cannot conclude with confidence that multiple star-formation events took place, because of the discrete and rather coarse age sampling of the model templates. The case for multiple episodes is thus strong only if model components of very different age are required to match the data. It may also be difficult to distinguish between contributions from a few-Myr-old stellar population and from an AGN power law, particularly in data with low SNR.

The resulting best fits are overplotted on the original spectra in Figure 1. In general the agreement with the data is quite good. The luminosity-weighted mean ages $\overline{T}_{light}$ of these models are given in Table 3, while their distribution is shown in the top panel of Figure 3. The $\overline{T}_{light}$ values have a median of 10^{10} yr, with 68% of the values around the median lying between $10^{9.39}$ and 10^{10} yr.

The age estimates produced in this analysis, which are conservative as lower limits, reinforce the conclusion from the single-age analysis that the majority (17/23) of our nuclear spectra are consistent with a stellar population considerably older than $10^{9.5}$ yr. Exceptions to this finding include the same sources identified as anomalies in §4.1, with in addition NGC 3489, NGC 3982, and NGC 4321. The impact of considering multiple instead of single templates on our age estimates is also shown in the middle panel of Figure 3. Allowing multiple templates has an impact on the estimated age only for those objects that require contributions from both old and young templates: the best single template appears to be systematically younger than the luminosity-weighted mean age of the present population mix.

Figure 4 shows four examples of how the inclusion of multiple single-age templates considerably improves the description of our data. The need for multiple templates is mostly dictated by the continuum shape, in that younger model components yield improvement in matching the blue end for some objects (e.g., NGC 4321, NGC 4203). Our models are, however, also very sensitive to strong absorption features in the spectra of the highest quality (NGC 3368, NGC 5055). The light weights for the contributing age components of each model are listed in Table 4 and shown graphically in Figure 5.

Although the models of Figure 1 would seem quite good, the χ^2_ν values listed in Table 3 suggest that in some cases the models are not altogether satisfactory. Several factors contribute to this situation.

The most common disagreement with the observations appears around the Mg b 5175 Å feature. The quality of the fit in this region appears to be correlated with the success in

fitting the CN-band absorption around 4200 Å; NGC 4800 is illustrative of a successful fit for the two features, while NGC 4459 shows noticeable deviations in both. This pattern suggests an α-enhancement in the chemical content of the nuclear stellar populations of many of these sources, and highlights the need for more sophisticated models accounting for non-solar abundance ratios. While the Mg b and CN features are some of the more obvious regions showing disagreement, they do not dominate the fit outcome. Exclusion of these regions alone from the fit does not substantially decrease the χ^2_ν values (the median value moves from 1.58 to 1.38) and also does not affect the derived population mixtures. Other weaker features are also a factor in the elevated χ^2 values.

The other most common source of deviation is found at the bluest ends of many of our spectra, where our models tend to be brighter than the data. In this regard we note two kinds of behavior. For some objects the shape of the blue continuum of our model appears approximately correct (e.g., NGC 4459, NGC 4477) while for others there is greater contrast and a divergence of the model and data at the blue end (e.g., NGC 4203, NGC 4450, and to a lesser degree in NGC 3982, NGC 4143). For most objects in the first class, the SED is already matched by the oldest, and reddest, template in our library, which, however, is still too blue in comparison with the data. Adding more dust extinction does not help, as it makes the model too red at the long-wavelength end. Another possibility is that a component of stars older than 10 Gyr is present. As an indicator of how this could change the spectrum, we note that for the same flux around 5700 Å, a 20-Gyr-old B&C template is roughly 20% fainter around 3000 Å than the 10-Gyr-old template. For the objects in the second class, on the other hand, a combination of old and young stars does a much better job than a single-age model in reproducing the overall continuum shape (e.g., see NGC 4203, Fig. 4); however, the required amount of $10^{6.5-7.5}$-yr-old stars still does not account for the blue continuum slope. For these objects, we suspect that a featureless continuum may contribute to their SEDs.

Finally, the STIS error arrays associated with the spectra may sometimes be underestimating the real uncertainties. This seems to be the case in particular for NGC 5055, where inspection of the model reveals an apparently quite good fit to the data (Fig. 4), yet $\chi^2_\nu = 10.45$; the formal errors seem to be smaller than the intrinsic scatter in the data. This situation does not affect our results, in that a global scale-factor offset in the error arrays does not influence what population mix provides the best fit; the relative weighting is unchanged. For each object, the error spectrum properly gives the lowest weight to the bluest part of the spectrum, where the data are noisiest.

4.2.2. Significance of Multiple Components

To quantify in more detail whether multi-age templates are really needed to describe these data, we considered the best-matching models using one template or using multiple templates as two particular configurations of the same model, with the single-template models being a nested realization where 10 of the light weights are set to zero. In this situation our two representations of the data would be consistent with each other if their χ^2 values would differ by less than the $+3\sigma$ confidence limit corresponding to a χ^2 distribution with a number of degrees of freedom equal to the number of free parameters in our models (see Theorem C of §15.6 of Press et al. 1986). If the χ^2 values differ by less than this amount, there is no need for multiple templates. Our models include 14 parameters, of which 2 describe the kinematics (V, σ), 1 describes the intrinsic reddening (A_V), and 11 are relative weights of the empirical templates. Although the problem is not linear in V, σ, and A_V, we assume that the number of data points is large enough for this approach to still be valid. In order to be as conservative as possible during this evaluation, we rescaled all χ^2 values assuming that our best multi-age models have χ^2 equal to the number of useful data points in our nuclear spectra minus the number of free parameters. In most of the present cases this procedure is equivalent to stating that the adopted errors are actually underestimates of the real uncertainties, which appear justified in light of the previous considerations.

Among the nuclei requiring multiple templates in Table 4, the difference between the χ^2 values for the best single-age and multiple-age models suggests a real need for a template mix in all of them except for NGC 4245 and NGC 4800. For NGC 4435, a closer comparison between the model differences and the error arrays suggests that the evidence for multiple components is also marginal. This analysis demonstrates in general that we are not sensitive to detection of distinct components with light fractions less than a few percent (see Table 4), depending on the quality of the spectra.

We can use these results to gauge the significance of the light and mass fractions of stars younger than 1 Gyr yr for our sample, which are also listed in Table 3. NGC 278 is confirmed to be the youngest nucleus in our sample, and is best explained with a single-age, $10^{8.5}$-yr-old template. Excluding the previously mentioned weak and marginal cases, the fits improve significantly for 9 out of 23 objects when contributions from stars younger than 1 Gyr are included, with flux fractions larger than 10% in 8 cases. For NGC 3489, the fraction of stars younger than 1 Gyr is less than 10%, but the large weight for the 1 Gyr template (Table 4) and the coarseness of our age grid leave open the possibility that we may be underestimating the fraction of stars younger than 1 Gyr. On the other hand, for NGC 3982, NGC 4143, NGC 4203, and NGC 4450, the poor match of the blue-continuum shape after introducing young stars suggests that their presence may be overestimated. Instead, the presence of AGN

continuum would be consistent with the signatures of broad lines (NGC 4143, NGC 4203, NGC 4450) or strong, high-excitation emission lines (NGC 3982) found in these objects. All of these nuclei also show very concentrated light profiles, reminiscent of unresolved central components (§4.4).

A better argument to rule out the presence of young stars in favor of a featureless continuum in these four objects would be to find evidence for dilution in the absorption-line features. In order to make our method more sensitive to the absorption features rather than to the continuum shape, we repeated our analysis including an additive, low-order polynomial component while solving for the template weights (step 2, §3), and suppressing the reddening correction. The polynomial introduces a considerably greater degree of flexibility for optimizing the overall continuum shape of the model, but its presence will tend to dilute the strength of narrow absorption lines, making it particularly suitable for revealing the presence of an AGN-like continuum component.

After refitting all spectra with this prescription, the main results of our analysis (i.e., light-weight distributions, luminosity-weighted mean age, and light-fraction of stars younger than 1 Gyr) turned out to be very similar to those obtained from our previous, best-reddened models. The only exceptions to this statement are exactly the same four targets where we already suspected that the presence of a featureless continuum is more likely than that of $\sim$1-Myr-old stars. With inclusion of the polynomial, only a very old population is needed to describe these nuclei, while the presence of young stars persists in all the other objects where the reddened models required them. This outcome suggests that for the latter spectra, and the others showing only old stellar populations, the polynomial adjustment simply acts as a substitute for interstellar reddening without affecting significantly the absorption-line strengths, while in NGC 3982, NGC 4143, NGC 4203, and NGC 4450 it is actually required by the data to mimic a blue featureless continuum and to dilute the absorption-line features.

Yet, it may be argued that allowing the youngest stellar component to be subjected to a larger amount of dust extinction than the rest of the stellar population, so as to mimic a dusty nuclear starburst, will also provide the needed correction for the continuum slope and dilution of the absorption features. We explored this possibility in the specific case of NGC 4203. We have modified our standard multi-component fit to produce two sets of models, one that allows for a different reddening of the youngest templates (< 100 Myr), and another that includes a featureless continuum represented by a power law with a slope that is free to vary and that is also subject to a different reddening. No polynomial components were used.

Fig. 6 shows the result of this experiment. Both heavily reddened O-stars and an AGN component can indeed offer almost identical continuum-shape corrections, which improve the

match to the blue end of the spectrum. Yet the young templates are not entirely featureless and the model with an AGN component can better explain the data in the spectral region before and after the Balmer break (between 3600 Å and 3850 Å). Although the presence of high-order Balmer emission lines filling the corresponding absorption features could mitigate this difference, the mismatch in the spectral region on the blue side of the [O II] λ3727 emission line remains larger for the model with young stars. Even if the difference between these two models is significant in a statistical sense, we consider that data with higher SNR are needed to convincingly separate the contribution of young stars from that of a featureless continuum in this wavelength range; for the objects where we suspect the presence of an AGN-like continuum, the strongest evidence for this component is therefore indirect, based on the other indications of an accretion source as noted above. We note that González-Delgado et al. (2004) similarly concluded that the presence of young stars is unlikely in these nuclei, and pointed out that using UV spectra is the best way to further investigate this issue (e.g., Heckman et al. 1997).

4.2.3. Other Considerations

In 2.1 we estimated that on average $\sim 40\%$ of the light in our spectra could originate from bulge stars, most likely very old ones (e.g., Peletier et al. 1999). If we assume that such contamination enters only in the fraction of light from 10-Gyr-old stars that we detect, than its impact on the light weights of Table 4 can easily be estimated by re-normalizing all light weights after decreasing the fraction of 10-Gyr-old templates by 0.4, or set them to zero when this is less than 40%. Although this would increase by $\sim 70\%$ all other light weights, the fractions of light from stars younger than 1 Gyr would change very little, increasing on average by only 0.05. The impact on the mass fraction would be even smaller.

We conclude this section by considering the amount of intrinsic dust reddening required by our models. The extinction values listed in Table 3 have an average $\overline{A}_V = 0.37$ mag and a standard deviation of 0.25 mag. This result is smaller than the typical $A_V = 0.6-1.0$ mag found by Peletier et al. (1999) through analysis of BIH colors measured from *HST* images of disk galaxy bulges. The origin of this discrepancy is not clear. Although the wavelength coverage of our spectra is much less than that of the broad-band observations of Peletier et al., we consider our A_V estimates to be fairly robust.[2] The information provided by detailed

[2]For our adopted A_V grid, models with A_V differing from the best-fit value invariably result in much worse χ^2; consequently the grid step of 0.1 can be considered a conservative estimate of the uncertainty in A_V.

spectral features in addition to the broader shape of the blue continuum means that our analysis is much less susceptible to uncertainties in the stellar population, while retaining considerable sensitivity to reddening.

One aspect of the bulge stellar populations that we have not yet addressed is the effect of different metallicity. Studies of abundance gradients in galaxy disks suggest that the regions we are studying may have very high metallicities (e.g., Vila-Costas & Edmunds 1992, and references therein). This issue is important in the context of determining A_V values, since super-solar metallicities result in redder intrinsic templates (see Fig. 2). A possibility is that the galaxy spectra are systematically redder than the solar metallicity templates in part because they have metallicities $Z > Z_\odot$, and not simply due to interstellar absorption. Use of nonsolar templates in the fitting process can also be expected to affect our estimates of $\overline{T}_{light}$ since age and metallicity are well known to be highly degenerate in their spectroscopic effects. We explore these issues in the following section.

4.3. Super-Solar Metallicity Models

In order to investigate the importance of enhanced metallicity in our sample nuclei, we repeated our multi-component analysis, including interstellar reddening, with B&C templates for super-solar metallicities, which are limited to $Z = 2.5Z_\odot$.

Table 5 lists these results; the corresponding $\overline{T}_{light}$ distribution is characterized by a median age of $10^{9.89}$ yr, with 16% and 84% percentiles of $10^{9.23}$ and 10^{10} yr, respectively. These values differ only slightly from the findings reported in §4.2. The bottom panel of Figure 3 further shows that for all but three objects, the $\overline{T}_{light}$ values shifted by less than 30% toward younger ages. In fact, the $\overline{T}_{light}$ values of Table 5 are on average only 10% younger than those of Table 3.

A comparison between the χ^2_ν values listed in these two tables shows that for all but two nuclei, the use of templates with super-solar metallicities always leads to a better description of the data, although the improvement is not always statistically significant. Figure 7 shows two examples of fits where the improvement resulting from use of the $2.5Z_\odot$ templates is notably strong (NGC 4459, NGC 4477), along with two examples where the improvement is more modest (NGC 4800, NGC 278). The case of NGC 4459 is particularly instructive in showing details that are better fit with the high-metallicity templates. The Mg b 5175 Å feature benefits from using these models; likewise, the whole region between 4400 Å and 4800 Å is better reproduced with the super-solar templates, in particular thanks to stronger Fe 4531 Å and Ca 4668 Å absorption lines. The high-metallicity templates are not sufficient

to explain the strength of the CN band around 4200 Å, however, consistent with the idea that this mismatch highlights the need for non-solar abundance ratios. Likewise, the $2.5Z_\odot$ templates cannot account for the discrepancies in the bluest regions of our spectra noted in §4.2, suggesting again that the oldest nuclei in our sample may have stellar populations older than 10 Gyr, or that in cases like NGC 4203 and NGC 4450 the presence of young stars may still be overestimated.

In Table 5 we list the summed light and mass fraction of stars younger than 1 Gyr for the super-solar models affording the best fits. Use of the high-metallicity templates does not change our conclusions concerning which nuclei show significant ($\gtrsim 10\%$) evidence for a young stellar component. The table also lists values for A_V, which, as expected, are lower than the $Z_\odot$ case, with $\overline{A}_V = 0.18 \pm 0.04$ mag. A suspicious aspect of the A_V distribution is the fact that 10 out of 23 nuclei are best fit with $A_V = 0$ mag. This finding suggests that the $Z = 2.5Z_\odot$ templates are actually *redder* than our spectra in many cases, which might imply that a metallicity of $2.5Z_\odot$ is too high. The fact that the detailed absorption features are better fit by the $2.5Z_\odot$ models while the overall continuum shape is apparently better represented by the $Z_\odot$ models suggests that we are encountering a fundamental limit in the accuracy to which the B&C models can be applied to the current problem. The results nonetheless allow us to conclude that typical metallicities fall within the interval of $(1\text{–}2.5)Z_\odot$ for the inner bulges of our sample galaxies.

4.4. Contribution from Nuclear Power-Law Sources or Young Star Clusters

Our multi-age fits indicate that a significant fraction of the nuclei in our sample have a component of very young (few-Myr old) stars, or alternatively, a featureless blue continuum component as may arise from an accretion source. In this section we present quantitative bounds on the contributions of such components along with their significance, evaluated by a $\Delta\chi^2$ analysis as in our study of multiple-age components (§4.2). We adopted as our fiducial description of the nuclear spectra the multi-age models with solar metallicity derived in §4.2.

For each object we obtained fits by fixing the fraction of total blue light f_{blue} contributed by a 10^6-yr-old population, and repeating the fit with different f_{blue} values to produce a model sequence. For a given fit, the relative contributions of the other age components and the common extinction value were left as free parameters. We then compared the results with the best fits, and derived $\pm 3\sigma$ confidence limits for f_{blue} as in §4.2, where in this case the χ^2 values follow a χ^2 distribution for one degree of freedom. The same approach was used to determine the best-fit contribution and 3σ bounds for a featureless continuum, which we represent by a power law with $f_\nu \propto \nu^{-\alpha}$ or $f_\lambda \propto \lambda^{\alpha-2}$. Our limited spectral baseline

makes it difficult to independently constrain α, and consequently we adopted a fixed value of $\alpha = 0.5$, which is representative of power-law slopes observed in luminous AGNs (e.g., Zheng & Malkan 1993). The fraction f_{blue} is calculated for the bandpass 3050–3200 Å, where a component of young stars or an AGN continuum is likely to be most prominent. In order to derive conservative bounds, we rescaled all χ^2 values as done is §4.2, which has the result of widening the calculated confidence limits.

The results, shown in Figure 8, indicate that the flux contribution from a "blue component" is very small ($\lesssim 10\%$) in roughly half of our nuclear spectra, regardless of the stellar or AGN nature.

A number of other nuclei (e.g., NGC 3982, NGC 4143, NGC 4203, and NGC 4450; see also §4.2) clearly require a non-zero AGN-like continuum (Fig. 8*a*). The presence of probable AGN continuum emission is in accord with the signatures of broad lines (NGC 4143, NGC 4203, NGC 4450) or strong, high-excitation emission lines (NGC 3982) found in the same objects. The fits also suggest that a young-star component is not strictly needed in NGC 3982, NGC 4143, NGC 4203, and NGC 4450. With such an AGN component these nuclei require only a 10 Gyr stellar population. In other objects an AGN-like continuum is perhaps needed, but the SNR is too low to be conclusive (NGC 3351, NGC 4321).

Excluding the probable AGNs (shown with dotted lines in Figure 8*b*), the 3σ maximum contribution from a 10^6-yr-old population has a median value of only 6% for the sample, which represents the sensitivity limit of our experiment for detecting such young stars. For comparison, in the case of our Milky Way we would not have been able to detect the light emitted by its young central clusters, as these contribute only $\sim 1\%$ of the light at ~ 3000 Å coming from the central 10 pc (D. Figer, 2003, private communication).

The STIS acquisition images for our target galaxies reveal that the objects requiring a featureless component all show a high degree of concentration in their nuclear surface brightness distribution. In the case of NGC 4203, this correspondence supports the exclusion of its central unresolved light component from the stellar budget while measuring its central SMBH mass (Shields et al. 2000; Sarzi et al. 2001). No such signature is apparent from inspection of images for sources with spectral fits implicating a Myr-old stellar population, with the exception of the youngest object in our sample, NGC 278, which displays a nuclear cluster like the ones discovered by Carollo, Stiavelli, & Mack (1998) and Böker et al. (2002). The work by Carollo et al. indicates that compact nuclear components can often be rather subtle in their photometric signature, and detection of these structures in images such as we have available can be seriously complicated by dust absorption. It is therefore possible that compact clusters are present in a large fraction of our sample galaxies; near-infrared images would be very helpful in addressing this issue.

We conclude this section by asking whether the upper limits on young stellar populations would be accompanied by emission of ionizing photons sufficient to explain the observed emission-line fluxes, collected either within the same *HST*-STIS aperture or by ground-based observations.

We used the 1-Myr model SEDs along with the derived upper limits on their blue light contribution to estimate the maximum production rate of ionizing photons in each source, in order to predict the Hα flux, by assuming that all ionizing photons are absorbed and that Case B recombination applies (Hummer & Storey 1987). This derivation includes the extinction correction for the blue continuum that we obtained from our fit, and assumes that a negligible fraction of the ionizing photons are intercepted by dust. The resulting predictions are thus conservative in estimating the *maximum* Hα fluxes that could plausibly result from H II regions powered by young stars. We finally applied to these hypothetical fluxes the foreground Galactic extinction along each object direction (Table 1). Table 6 lists the theoretical predictions from this exercise along with the observed Hα fluxes observed in our G750M spectra. The Hα measurements were obtained after subtraction of the stellar continuum as part of a larger study of the nebular properties of the sample nuclei presented by Shields et al. (2004b). The listed Hα fluxes have not been corrected for extinction internal to the source galaxy. Reddening estimates from the measured Hα/Hβ ratio and recombination theory are available for fewer than half of our target nuclei because of limitations in the data.[3] By neglecting internal extinction of Hα, we are again conservative in gauging the extent to which something other than stars is required to power the nebular emission. A comparison of the resulting predicted versus observed Hα fluxes is shown graphically in Figure 9, where the emission-line classification derived from ground-based observations (Ho, Filippenko, & Sargent 1997) is indicated by the symbol type.

It is important to keep in mind that H II regions can be subject to large amounts of extinction, up to several magnitudes (e.g., Rodríguez 1999). More O-stars could thus be present in these nuclei without being detected, if they are substantially more obscured than the rest of the stellar population. However, such deeply embedded stars would not contribute significantly to the ionizing flux powering the observed nebulosity unless the geometry were fine-tuned so that the stars were obscured only along our line of sight.

Figure 9 shows results that are generally consistent with our expectations for the role of accretion power, as indicated by the emission-line classification of the nuclei. For three of the

[3]Studies of other star-forming galaxies indicate that reddening of the optical nebular emission is generally comparable to or somewhat greater than that of the associated blue starlight (e.g., Calzetti 1997), and this behavior is weakly confirmed in our data.

four Seyfert nuclei in our sample, the observed Hα flux exceeds the predicted contribution from young stars, and the same statement probably applies to the fourth object, NGC 3982, since as noted earlier the young stellar component is likely overestimated in this source. Two of the LINER 1 nuclei (NGC 4203, NGC 4450) are formally consistent with ionization by stars, although the allowed flux from young stars is again probably overestimated; consistency with stellar photoionization is at best marginal for the remaining two LINER 1s (NGC 2787, NGC 4143) under the current optimistic assumptions. A majority of the LINER 2s also show only marginal consistency with starlight as the sole source of ionization. The situation is mixed for the transition sources: two are consistent with stellar photoionization, two are probably not, and a further two are indeterminate because of upper limits in both coordinates. The H II nuclei that are detected in Hα are consistent with ionization by hot stars.

Considering that the emission-line fluxes obtained in ground-based measurements (Ho, Filippenko, & Sargent 1997) over apertures an order of magnitude larger in radius contain 10–100 times as much emission as measured here (see Shields et al. 2004a), none of these galactic nuclei contain enough very young stars in their central $\sim$ 10 pc to explain the nebular luminosity observed over $\sim$ 100 pc scales. The upper limits for the power law shown in Figure 7*b*, however, translate into ionizing photon production rates that exceed the large-scale nebular requirements by a factor of 100 or more, when a simple extrapolation of the continuum is assumed. The real production rate will be very sensitive to the details of the continuum shape, but in general we can conclude that an accretion-powered continuum can in principle account for the nebular luminosity in these nuclei.

5. Discussion

The analysis described above indicates that the majority of stars within the central few tens of pc in our sample galaxies are many Gyr old. These results provide some new insights into the histories of galaxy nuclei. If our limited sample is representative of galaxy bulges, the majority of the current stellar mass in the central parsecs was assembled into stars $\sim 10^{10}$ yr ago, and little star formation has occurred subsequently. Quantitatively, if we adopt a relatively high value of 2% (Table 3) for the present mass fraction of stars younger than 1 Gyr as representative of star formation over the intervening time, then at most 20% of the nuclear stellar mass could have been built in the last 10 Gyr. The bulk of the stars thus formed at an epoch similar to, or somewhat earlier than, that of the "quasar era" ($z \approx 2$–3). This inference is in accord with quasar metallicity studies indicating that luminous accretion episodes are accompanied or preceded by vigorous star formation (Hamann & Ferland 1999),

and hence consistent with a picture wherein the formation processes of galaxy spheroids and SMBHs are tightly linked.[4]

A possible explanation for the lack of substantial younger populations may be advanced by considering impediments to star formation in close proximity to a SMBH. The tidal radius is $r_t \approx R_{cloud}(M_{\rm BH}/M_{cloud})^{1/3} \approx (M_{\rm BH}/\rho_{cloud})^{1/3}$, and the densities within the inner few-pc molecular regions of our Galaxy are $n_{\rm H_2} = 10^4 - 10^7\,{\rm cm}^{-3}$ (Morris & Serabyn 1996). If these values are typical of other galaxies, even the densest components will be subject to strong tidal limitations. For example, a molecular cloud core with $n_{\rm H_2} = 10^7\,{\rm cm}^{-3}$ would be torn apart if wandering closer than 7.3 pc from a $10^8\,{\rm M}_\odot$ SMBH.

Our spectroscopic findings are in general accord with the results of *HST* imaging surveys by Peletier et al. (1999) and Carollo et al. (2001, 2002). Peletier et al. find that bulge nuclei are substantially obscured by dust and very seldom show blue colors, and although the samples of Carollo et al. include only spiral galaxies, our results are also consistent with their interpretation of their color-color diagrams as showing that most of the nuclei look mildly obscured by dust and are at least 1 Gyr old. Our spectroscopic analysis suggests that interstellar reddening may be less than reported by Peletier et al.

In terms of morphology, Carollo, Stiavelli, & Mack (1998) find that $\sim 50\%$ of spiral galaxies contain a distinct nuclear component. An interesting question is whether these structures correspond to sites of recent star formation. We cannot directly test this idea due to the limitations of our imaging data for the present sample. However, we can use the upper limits on young stars from our spectra to compute corresponding broad-band magnitude limits, in order to gauge whether we are sensitive to the types of clusters found in previous work. A conservative threshold corresponding to detection of a 1-Gyr component providing 10% of the total measured starlight for one of our sample galaxies translates on average to a maximum detectable absolute V magnitude of -10. Although the distinct nuclei found by Carollo et al. often extend beyond the 8 pc radius typically subtended by our observations, the vast majority of the published nuclei are much brighter than $M_V = -10$ mag, suggesting that we can detect such components if they are indeed 1 Gyr old. The fact that the fraction of spiral galaxies with distinct nuclear components ($\sim 50\%$) is rather similar to that of our spirals showing strong indications for the presence of stars younger than 1 Gyr (5/14) suggests that these objects could in fact contain young stellar clusters. The fraction of nuclei with young stars is lower for our lenticular galaxies (1/9), although this may reflect

[4]Here and in the remainder of this discussion we excluded from the objects containing stars younger than 1 Gyr those nuclei where the formal presence of young stars suggested by our multiple-component analysis is either overruled by indirect evidence of a power law (NGC 3982, NGC 4143, NGC 4203, NGC 4450), or just marginal (NGC 4435).

a different sensitivity limit for this galaxy type. For a given cluster luminosity the degree of contrast between the cluster and its surroundings will be reduced in early-type galaxies with large bulges; the problem is exacerbated by the fact that bulges tend to have cuspy surface brightness profiles.

Star clusters will also tend to be luminous when younger, which would aid in their identification in imaging. This phenomenon is manifested in the case of NGC 278, which is unique in our sample for its prominent Balmer-dominated spectrum and distinct nuclear component in surface photometry, both consistent with a recently formed cluster. A more general phenomenon of recurrent star formation associated with a nuclear cluster, resulting in variation in the prominence of spectroscopic signatures of young stars, would be in accord with recent studies of late-type disk galaxies by Böker et al. (2002) and Walcher et al. (2004). Their work indicates that nuclear star clusters are common in such galaxies, that the clusters frequently exhibit spectroscopic signatures of young stars, and that the masses and detailed spectral properties are consistent with multiple episodes of star formation. The discovery of these clusters and the study of their stellar population is aided in these systems by the absence of a significant bulge.

Although signatures of young stars are found with somewhat greater frequency in spirals compared with lenticulars in our sample, there is not a strong correlation between the presence or strength of these components and Hubble type considered alone. Likewise, there is no correlation with stellar velocity dispersion or galaxy luminosity. However, other aspects of our sample reinforce the picture that contamination by bulge light is an important limiting factor for the detection of young nuclear clusters. Specifically, we note that the only S0 galaxy with detected young stars is our closest object, while the most distant galaxy with young stars belongs to the latest Hubble type in our sample (Sbc). As a group, then, the galaxies found to be hosting stars younger than 1 Gyr in their nuclei tend to be closer than the other objects in our sample, with a mean distance of 9.7 Mpc as opposed to 15.2 Mpc.

Interestingly, the presence of a component of stars younger than 1 Gyr appears connected also to the emission-line classification of the nucleus (Fig. 10), where the classifications are those listed in Table 1; for objects with dual classifications (NGC 3489, NGC 4435), we adopt the type listed first, which is marginally preferred. Evidence of young stars is found in H II, transition, and LINER 2 nuclei, but not in LINER 1s or Seyferts. As discussed in §4.2 and §4.4, some LINER 1s and Seyferts do show evidence of excess blue light (NGC 3982, NGC 4143, NGC 4203, NGC 4450), but this component is probably best described by a nonstellar power law rather than by young stars. The remaining LINER 1s and Seyferts are best fit by a purely old stellar population (NGC 2787, NGC 4477, NGC 4501, NGC 4698). This result is consistent with a picture in which Seyferts and the majority of LINERs are

accretion-powered systems. The association of young populations with transition or LINER 2 classifications suggests that stellar phenomena may have some role in influencing the observed nebular emission, although the results in Figure 9 imply that energetic processes other than simply photoionization by O-type stars would have to be involved. Another noteworthy aspect of Figure 10 is the fact that the majority of H II nuclei do *not* show evidence for young stars in the *HST* aperture. Star formation in these objects apparently occurs primarily in circumnuclear regions subtended by the larger apertures ($\sim$ 100 pc) characteristic of ground-based observations, and this picture is confirmed by spatial measurements of the nebular emission (Shields et al. 2004a). Our findings suggest that this could be the case also for Seyfert 2 nuclei, for which evidence of a $\sim$100-Myr-old stellar population at $\sim$100 pc scales has been reported in a number of cases (e.g., Schmitt, Storchi-Bergmann, & Fernandes 1999). The existence of a connection between the presence of young stars and the emission-line classification is consistent with the results of Gonzáles-Delgado et al. (2004), who find that the incidence of young stars in weak-[O I] low-luminosity AGNs ([O I]/H$\alpha \leq 0.25$) is larger than in strong-[O I] nuclei.

6. Conclusions

We have fitted stellar population templates to interpret the spectra for the inner $\sim$ 10 pc of a sample of galaxies with a variety of Hubble types and nuclear emission classifications. The primary result of our analysis is that the large majority of nuclei have spectral energy distributions consistent with simply old stellar populations. Only one object out of 23 is dominated by a young cluster of stars less than 1 Gyr old, which is also photometrically distinct. When using multi-age population fits to reflect more complex formation histories, we find a distribution of luminosity-weighted mean ages across the sample that is strongly peaked around 10 Gyr. This result persists if we account for dust reddening and super-solar metallicities as contributors to or possible alternative explanations for the quite red observed spectra. For most sample galaxies, only negligible amounts of stars can have formed in the central 10 pc during the second half of the Universe's life.

There is, however, a significant fraction of galactic nuclei that show modest amounts of young stars: evidence for stars younger than 1 Gyr is found in $\sim$ 25% of the cases. Very young stars, $\sim$ 1 Myr, are not required by the spectral template fits for any object, and their possible contribution to the flux at the blue end of our spectra ($\sim$ 3100 Å) is limited to less than 6% on average. With these upper limits, the production of ionizing photons by very young stars falls short of the requirements for powering the nebular emission in the central 10 pc of the Seyfert nuclei and most of the LINERs in our sample. Furthermore, none of these

23 galactic nuclei contain enough very young stars to explain the nebular luminosity observed over $\sim$ 100 pc scales, as typically observed from the ground. This shortfall of stellar UV photons holds true regardless of internal dust extinction. The presence of a young population ($\lesssim$1 Gyr) appears, however, correlated with the classification of the emission-line ratios.

In Seyferts and most LINERs our findings are naturally explained, if ionization comes largely from AGN accretion, not stars. For H II nuclei, our results imply that much of the central star formation is actually circumnuclear — it occurs in the range of a few 10 pc to a few 100 pc.

We note in closing that even for nearby galaxies at *HST* resolution, the contamination from stars in the central portion of the surrounding bulge is an important limiting factor. We could not have detected a quantity of young stars as small as found at the center of the Milky Way.

M.S. is grateful to Don Figer, Harald Kuntschner, John Magorrian, Dan McIntosh, Reynier Peletier, Mark Whittle, and Sukyoung Yi for their suggestions. This work was supported financially through NASA grants GO-07361 and GO-09788 from the Space Telescope Science Institute (STScI), which is operated by AURA, Inc., under NASA contract NAS 5-26555. Research by A.J.B. is supported by NASA through Hubble Fellowship grant #HST-HF-01134.01-A awarded by STScI. The work of L.C.H. is supported by the Carnegie Institution of Washington.

REFERENCES

Barth, A. J., Ho, L. C., & Sargent, W. L. W. 2002, AJ, 124, 2607

Böker, T., Laine, S., van der Marel, R. P., Sarzi, M., Rix, H.-W., Ho, L., & Shields, J. C. 2002, AJ, 123, 1389

Böker, T., van der Marel, R. P., Mazzuca, L., Rix, H.-W., Rudnick, G., Ho, L. C., & Shields, J. C. 2001, AJ, 121, 1473

Böker, T., van der Marel, R. P., & Vacca, W. D. 1999, AJ, 118, 831

Bruzual, G., & Charlot, S. 2003, MNRAS, 344, 1000

Calzetti, D. 1997, AJ, 113, 162

Cardelli, J. A., Clayton, G. C., & Mathis, J. S. 1989, ApJ, 345, 245

Carollo, C. M., Stiavelli, M., & Mack, J. 1998, AJ, 116, 68

Carollo, C. M., Stiavelli, M., de Zeeuw, T. P., Seigar, M. & Dejonge, E. 2001, ApJ, 546, 216

Carollo, C. M., Stiavelli, M., Seigar, M., de Zeeuw, T. P., & Dejonge, E. 2002, ApJ, 123, 159

Colina, L., González-Delgado, R., Mas-Hesse, J. M., Leitherer, C., & Jiménez Bailón, E. 2002, ApJ, 579, 545

Corsini, E. M., et al. 1999, A&A, 342, 671

Dalle Ore, C., Faber, S. M., Jesus, J., Stoughton, R., & Burstein, D. 1991, ApJ, 366, 38

Di Nella, H., Garcia, A. M., Garnier, R., & Paturel, G. 1995, A&AS, 113, 151

Filippenko, A. V., in Active Galactic Nuclei: From Central Engine to Host Galaxy, ed. S. Collin, F. Combes, and I. Shlosman (San Francisco: Astron. Soc. Pacific), 369

Filippenko, A. V., & Sargent, W. L. W. 1985, ApJS, 57, 503

Filippenko, A. V., & Terlevich, R. 1992, ApJ, 397, L79

Genzel, R., et al. 2003, ApJ, 594, 812

González-Delgado, R. M., Heckman, T., Leitherer, C., Meurer, G., Krolik, J., Wilson, A. S., Kinney, A., & Koratkar, A. 1998, ApJ, 505, 174

González-Delgado, R. M., Cid Fernandes, R., Pèrez, E., Martins, L. P., Storchi-Bergmann, T., Schmitt, H., Heckman, T., & Leitherer, C. 2004, ApJ, 605, 127

Hamann, F., & Ferland, G. 1999, ARA&A, 37, 487

Heckman, T. M. 1980, A&A, 87, 152

Heckman, T. M., González-Delgado, R., Leitherer, C., Meurer, G. R., Krolik, J., Wilson, A. S., Koratkar, A., & Kinney, A. 1997, ApJ, 482, 114

Heckman, T. M., Robert, C., Leitherer, C., Garnett, D. R., & van der Rydt, F. 1998, ApJ, 503, 646

Héraudeau, Ph., & Simien, F. 1998, A&AS, 133, 317

Héraudeau, Ph., Simien, F., Maubon, G., & Prugniel, P. 1999, A&AS, 136, 509

Ho, L. C., Filippenko, A. V., & Sargent, W. L. W. 1993, ApJ, 417, 63

Ho, L. C., Filippenko, A. V., & Sargent, W. L. W. 1997, ApJS, 112, 315

Ho, L. C., Filippenko, A. V., & Sargent, W. L. W. 2003, ApJ, 583, 159

Ho, L. C., Rudnick, G., Rix, H.-W., Shields, J. C., McIntosh, D. H., Filippenko, A. V., Sargent, W. L. W., & Eracleous, M. 2000, ApJ, 541, 120

Hummer, D. G., & Storey, P. J. 1987, MNRAS, 224, 801

Jarvis, B. J., Dubath, P., Martinet, L., & Bacon, R. 1988, A&AS, 74, 513

Kent, S. M. 1990, AJ, 100, 377

Krabbe, A., et al. 1995, ApJ, 447, L95

Kuntschner, H. 2000, MNRAS, 315, 184

Lauer, T. R., Faber, S. M., Ajhar, E. A., Grillmair, C. J., & Scowen, P. A. 1998, AJ, 116, 2263

Maoz, D., Barth, A. J., Sternberg, A., Filippenko, A. V., Ho, L. C., Macchetto, F. D., Rix, H.-W., & Schneider, D. P. 1996, AJ, 111, 2248

Matthews, L. D., et al. 1999, AJ, 118, 208

Morris, M., & Serabyn, E. 1996, ARA&A, 34, 645

Peletier, R. F., Balcells, M., Davies, R. L. D., Andredakis, Y., Vazdekis, A., Burkert, A., & Prada, F. 1999, MNRAS, 310, 703

Press, W. H., Flannery, B. P., Teukolsky, S. A., & Vettering, W. T. 1986, Numerical Recipes: the Art of Scientific Computing (Cambridge: Cambridge Univ. Press)

Phillips, A. C., Illingworth, G. D., MacKenty, J. W., & Franx, M. 1996, AJ, 111, 1566

Rees, M. J. 1984, ARA&A, 22, 471

Rix, H.-W., Kennicutt, R. C., Braun, R., & Walterbos, R. A. M. 1995, ApJ, 438, 155

Rodríguez, M. 1999, A&A, 351, 1075

Salpeter, E. E. 1955, ApJ, 121, 161

Sarzi, M., Rix, H.-W., Shields, J. C., Rudnick, G., Ho, L. C., McIntosh, D. H., Filippenko, A. V., & Sargent, W. L. W. 2001, ApJ, 550, 65

Schlegel, D. J., Finkbeiner, D. P., & Davis, M. 1998, ApJ, 500, 525

Schmitt, H. R., Storchi-Bergmann, T., & Fernandes, R. C. 1999, MNRAS, 303, 173

Shields, J. C., Rix, H.-W., McIntosh, D. H., Ho, L. C., Rudnick, G., Filippenko, A. V., Sargent, W. L. W., & Sarzi, M. 2000 ApJ, 534, L27

Shields, J. C., et al. 2004, in Carnegie Observatories Astrophysics Series, Vol. 1: Coevolution of Black Holes and Galaxies, ed. L. C. Ho (Pasadena: Carnegie Observatories) (http://www.ociw.edu/ociw/symposia/series/symposium1/proceedings.html)

Shields, J. C., Rix, H.-W., Barth, A. J., Filippenko, A. V., Ho, L. C., McIntosh, D. H., Rudnick, G., Sargent, W. L. W., & Sarzi, M. 2004 ApJ, submitted.

Simien, F., & Prugniel, P. 1997, A&AS, 126, 519

Vazdekis, A. 1999, ApJ, 513, 224

Walcher, C. J.,vvan der Marel, R. P., McLaughlin, D., Rix, H.-W., Böker, T., Häring, N., Ho, L. C., Sarzi, M., & Shields, J. C. 2004, ApJ, in press., astro-ph/0409216

Vila-Costas, M. B., & Edmunds, M. G. 1992, MNRAS, 259, 121

Whitmore, B. C., Schechter, P. L., & Kirshner, R. P. 1979, ApJ, 234, 68

Worthey, G. 1994, ApJS, 95, 107

Worthey, G., & Ottaviani, D. L. 1997, ApJS, 111, 377

Zheng, W., & Malkan, M. A. 1993, ApJ, 415, 517

.

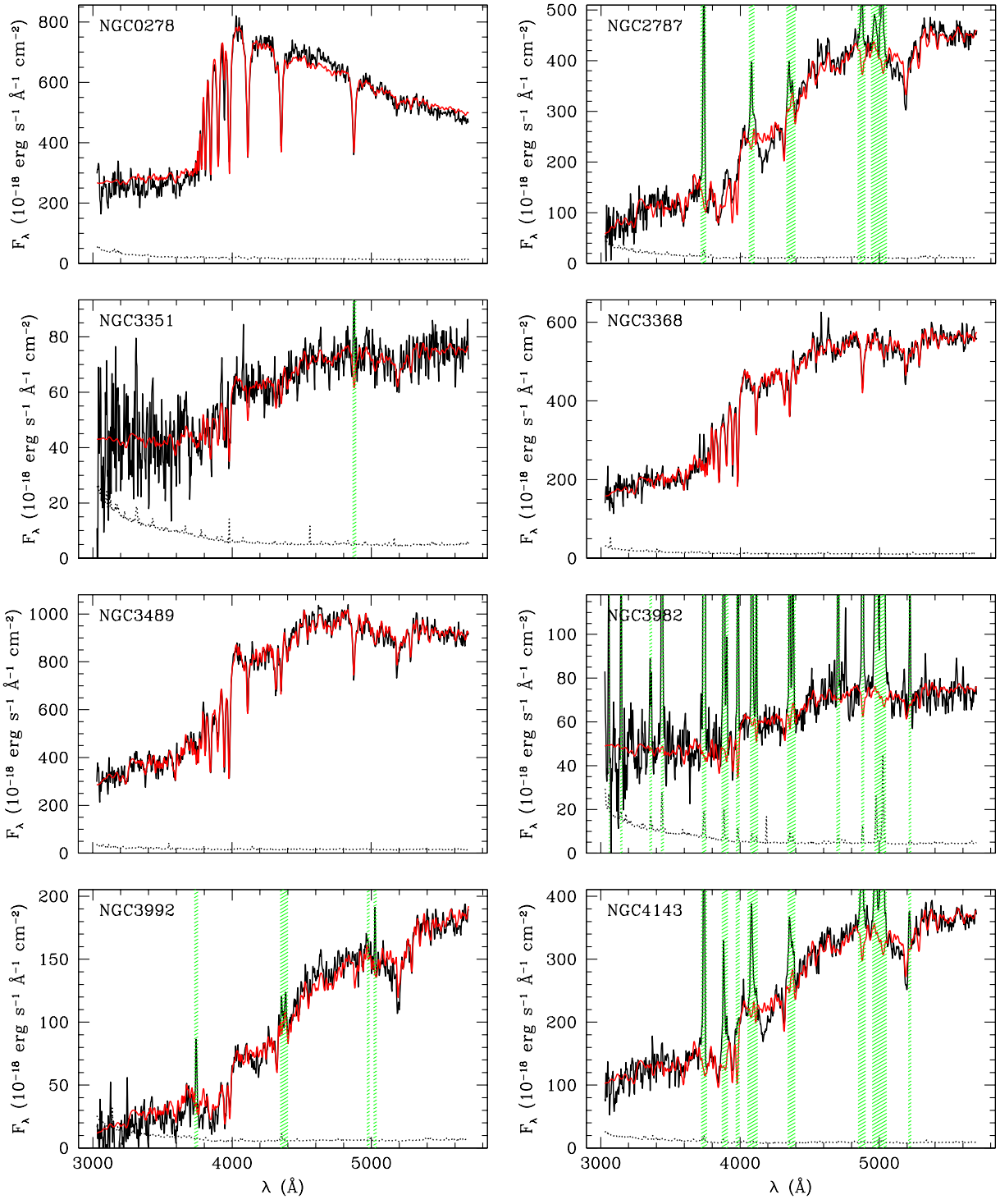

Fig. 1.— Nuclear G430L spectra extracted from the central $0\farcs25 \times 0\farcs2$ of our sample galaxies. The *dotted lines* at the bottom of each panel show the error array corresponding to the observed fluxes, while the *dashed green columns* indicate the spectral regions excluded during our analysis in order to avoid emission lines. The *red lines* show our best-fitting multiple-starburst population models. The observed fluxes have been corrected for Galactic foreground extinction, while the models account for dust extinction intrinsic to the source.

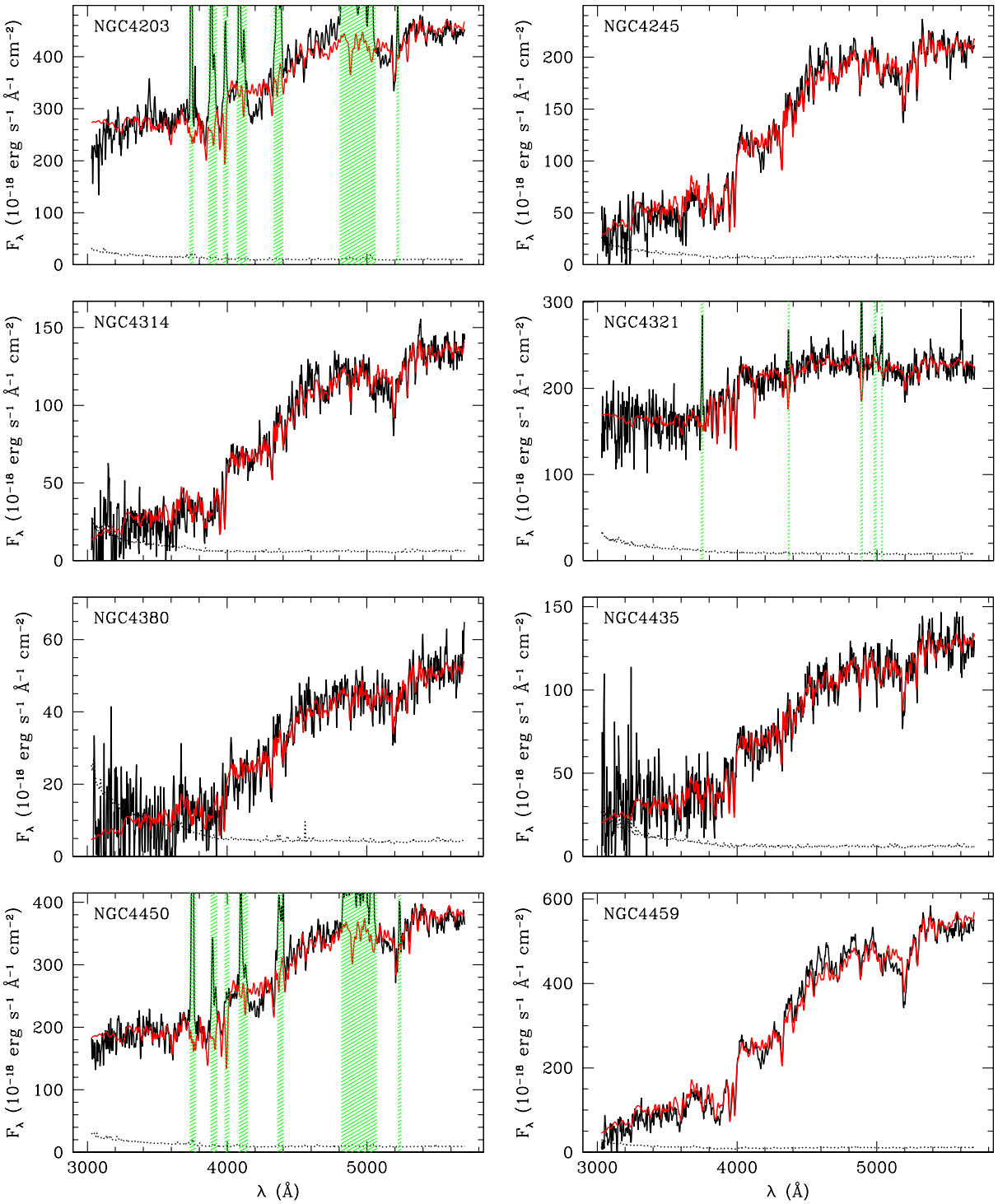

Fig. 1.— Continue

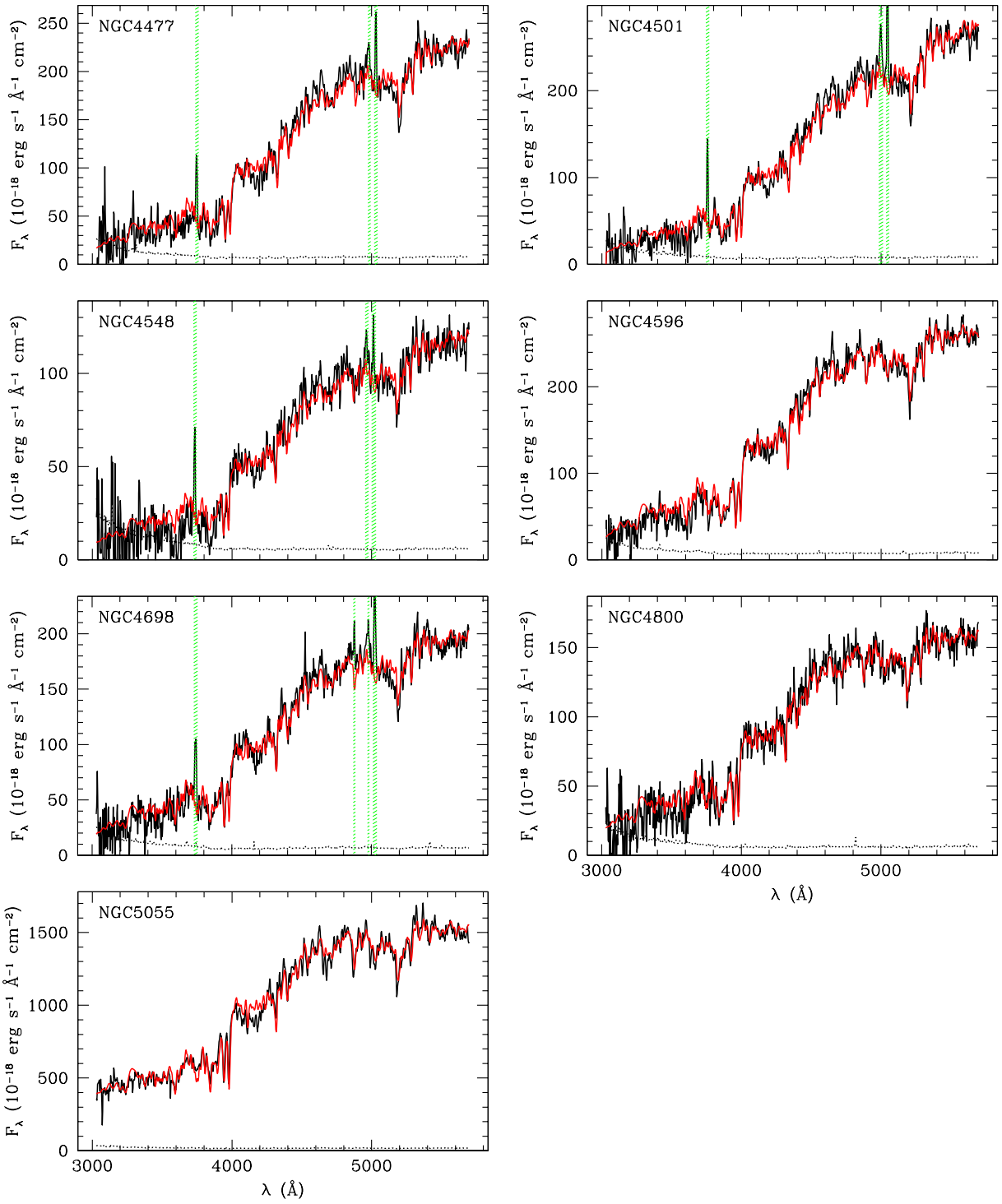

Fig. 1.— Continue

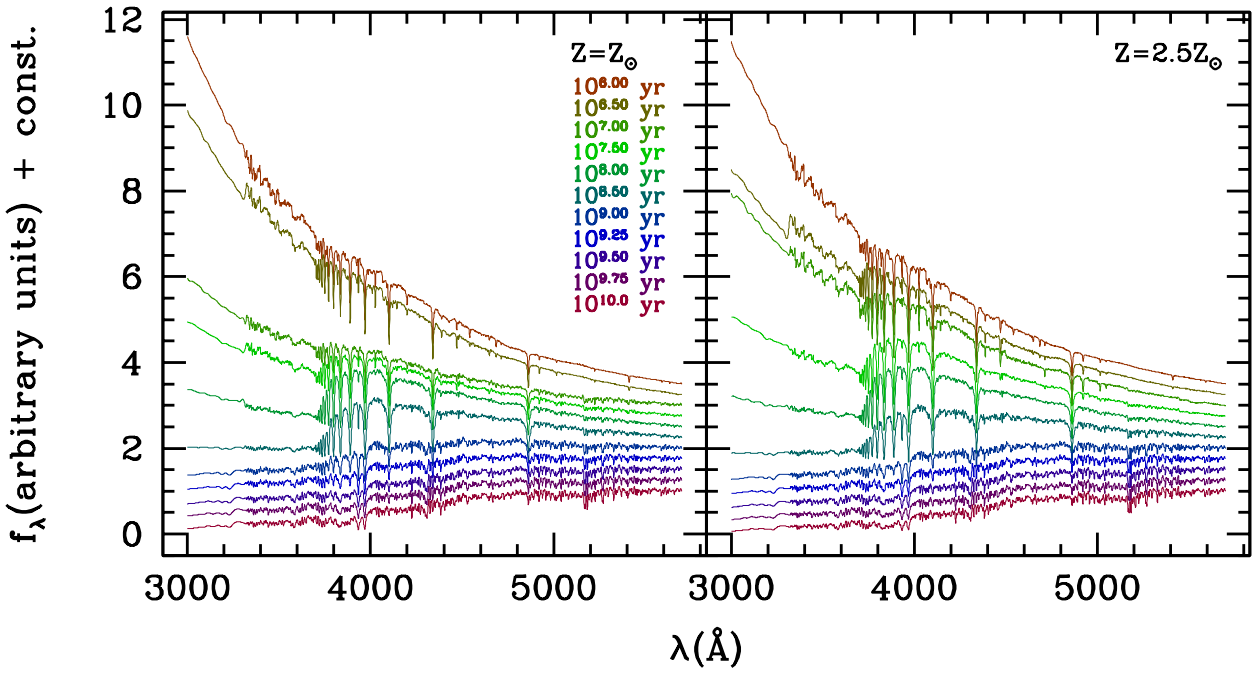

Fig. 2.— Bruzual & Charlot (2003) model SEDs for single-starburst stellar populations of different ages and solar (*left*) or 2.5 times solar (*right*) metallicities. The models are shown for the wavelength range matching our data, and for convenience of display they are normalized at 5700 Å and offset by a constant.

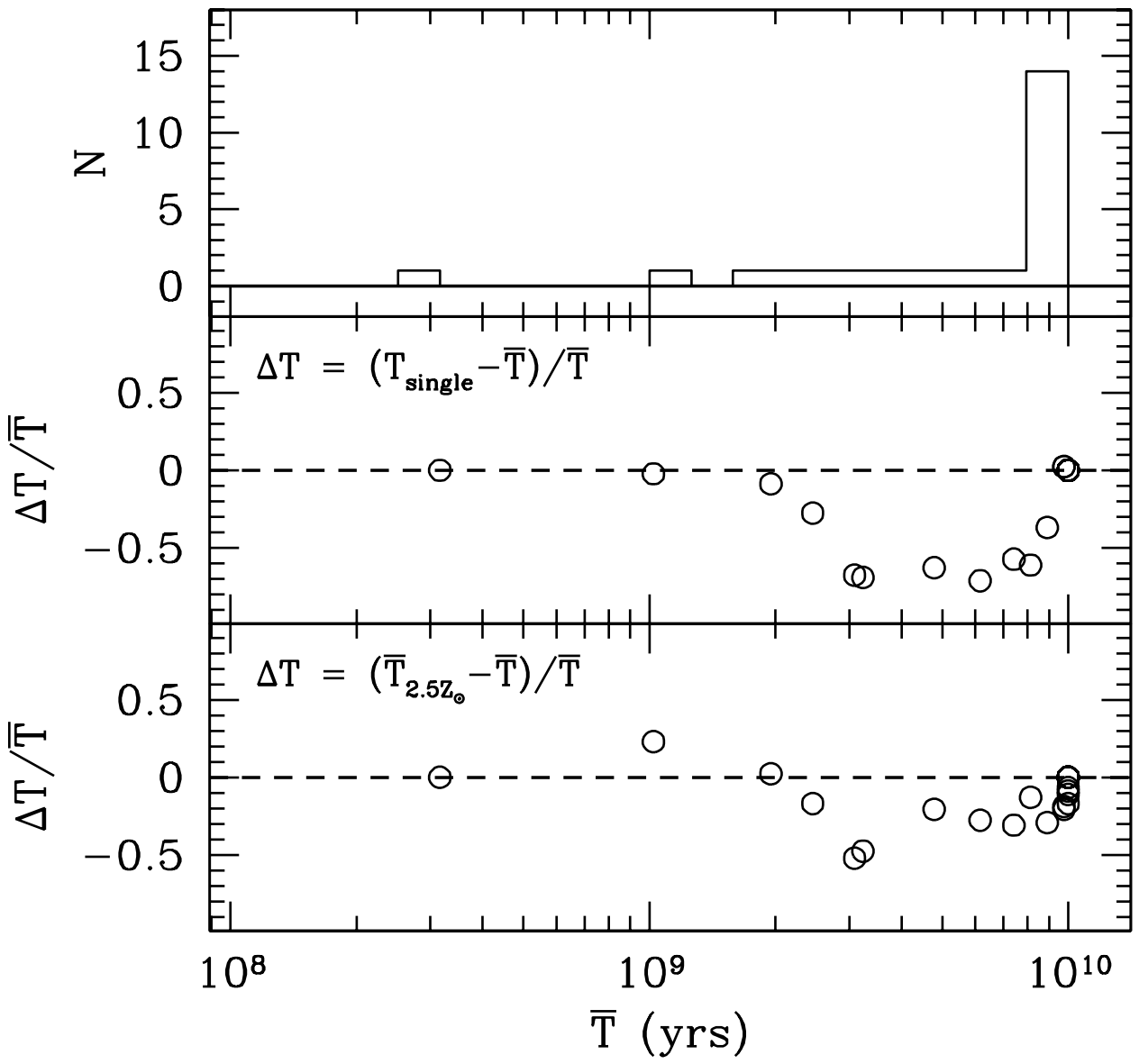

Fig. 3.— Distribution of the luminosity-weighted age estimates obtained from the best-fitting multiple-starburst models (*top panel*), which are also compared to the age of the best single-age models of §4.1 (*middle panel*) and the luminosity-weighted ages of §4.3, from multiple-starburst models of super-solar metallicity (*bottom panel*).

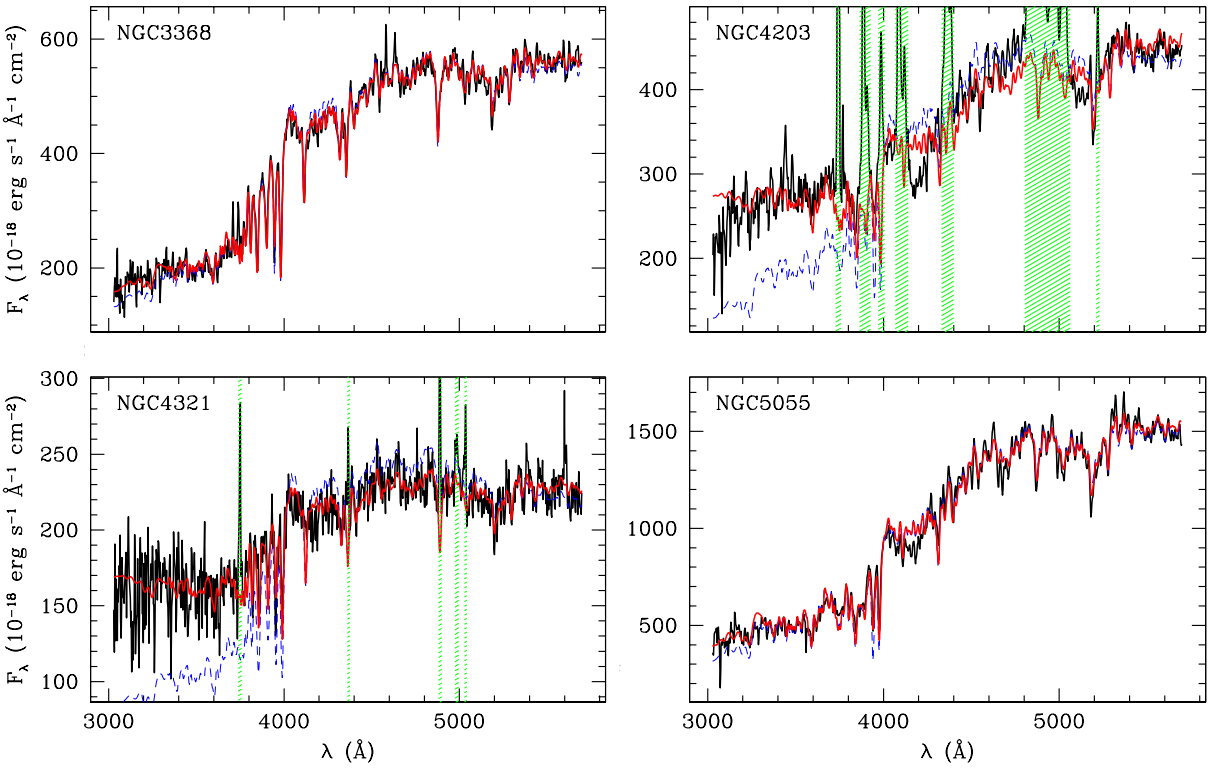

Fig. 4.— Examples of fits obtained with multiple-starburst models (*red lines*) versus single-age models (*blue dashed lines*).

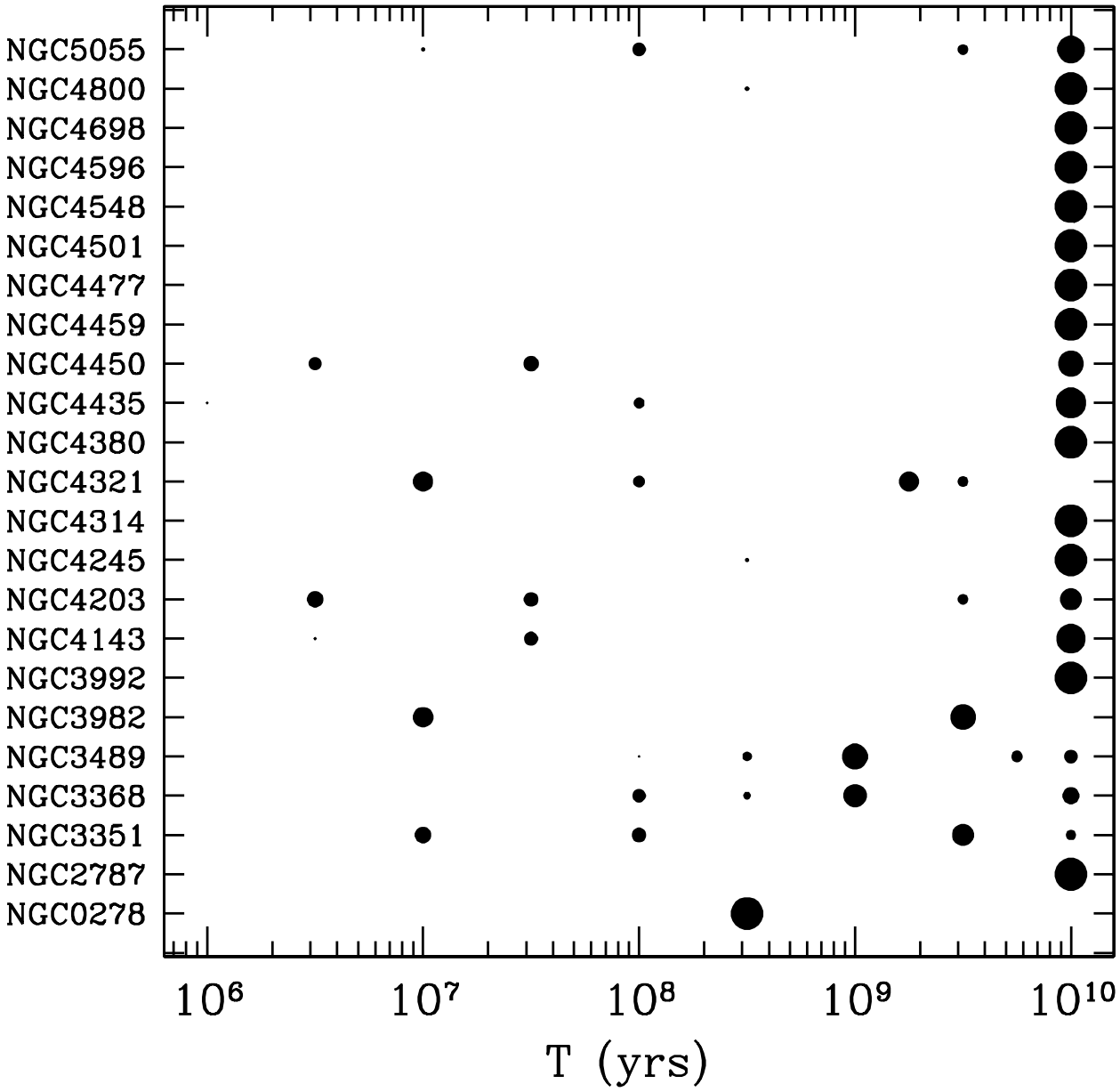

Fig. 5.— Graphical visualization of the relative light contribution of each single-age model to the best multiple-starburst models. The area of the *filled dots* is directly proportional to the relative weights listed in Table4.

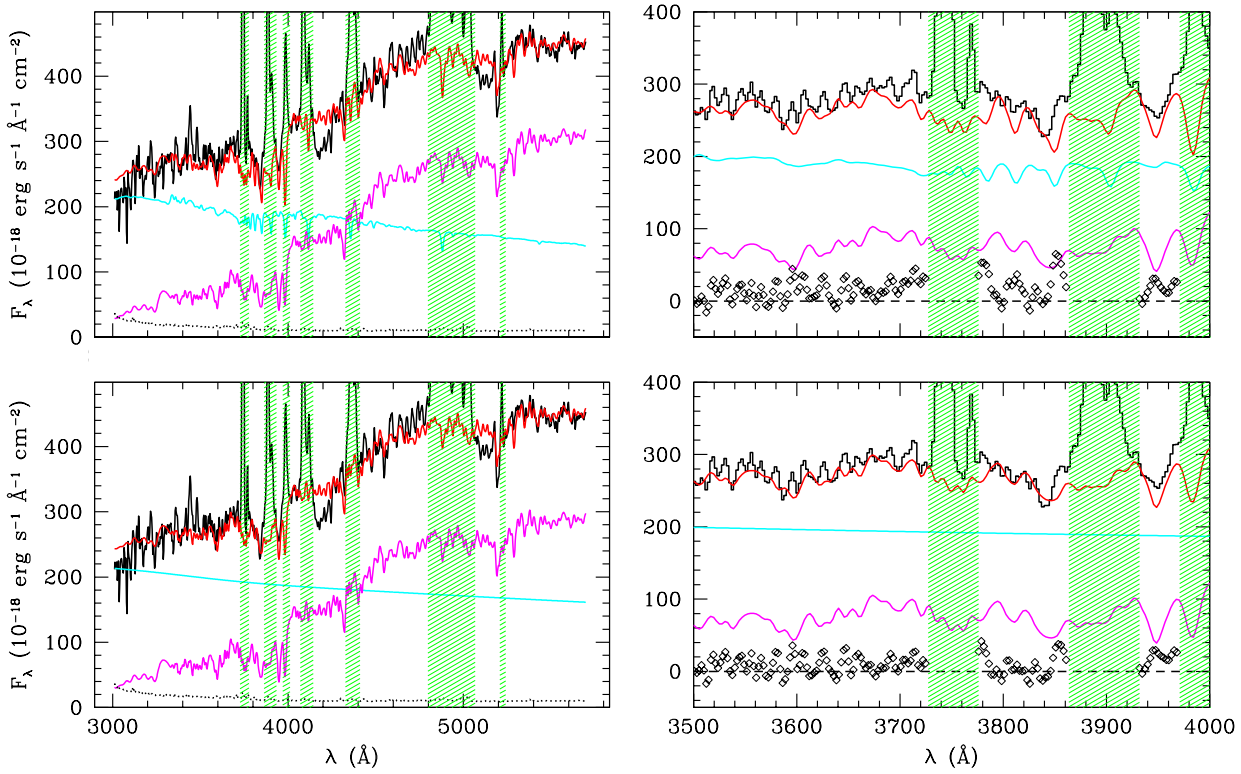

Fig. 6.— Young stars vs. AGN continuum in NGC 4203. *Left panels*: As for Fig. 1 but now showing separately also the contribution of intermediate-old populations (*purple lines*) and of either young stars (< 100 Myr, *top panels, light-blue lines*) or of the best power-law continuum (*bottom panels, light-blue lines*). Both young stars and featureless continuum are allowed to be subject to a different amount of dust extinction than the rest of the stellar population. *Right panels*: As in the left panels, but now showing the fits in the wavelength region on either side of the Balmer break, with the corresponding residuals (*diamonds*). The model with independently reddened young stars requires them to be subjected to a considerable amount of extinction ($A_V = 2.2$ mag) and to contribute 55% of the light (from the 3.2-Myr-old template). The model with an AGN continuum needs only 10-Gyr-old stars in addition to a power-law with slope $\alpha = 1.3$ reddened by $A_V = 0.2 mag$

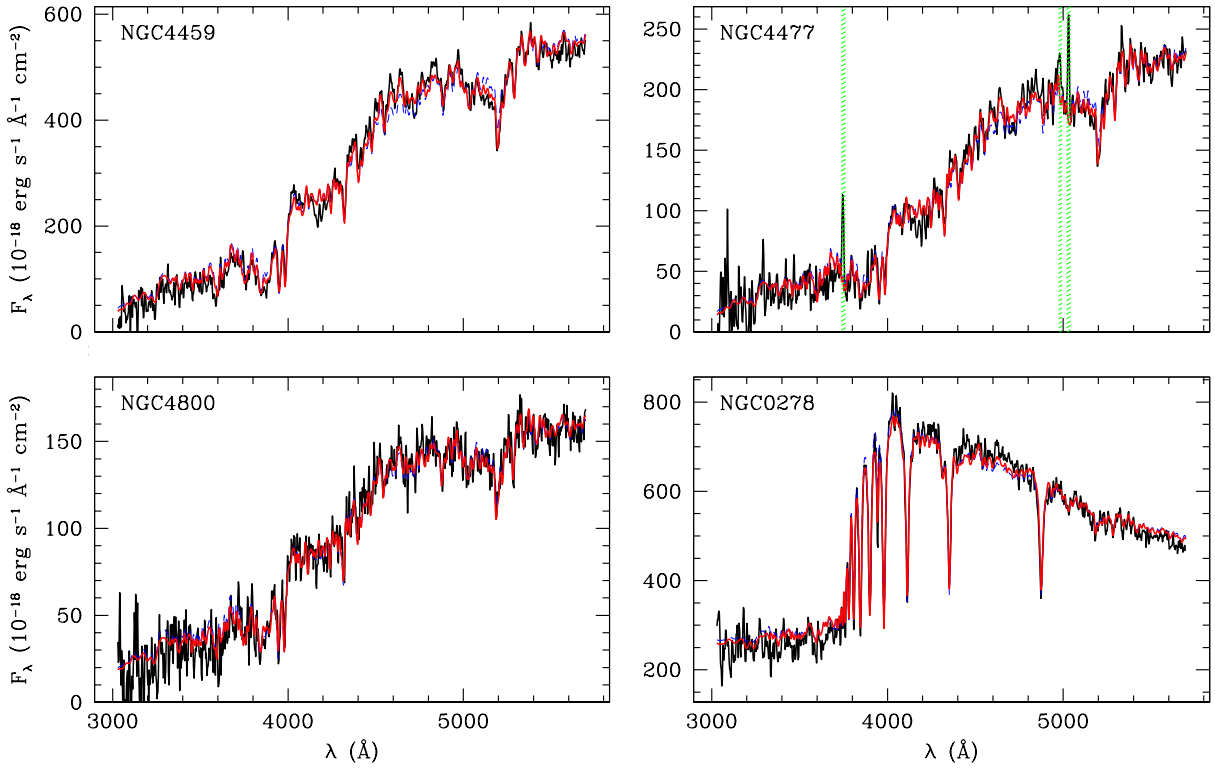

Fig. 7.— Examples of multiple-starburst models with super-solar ($Z = 2.5Z_{\odot}$, *red lines*) or solar ($Z = Z_{\odot}$, *blue dashed lines*) metallicity.

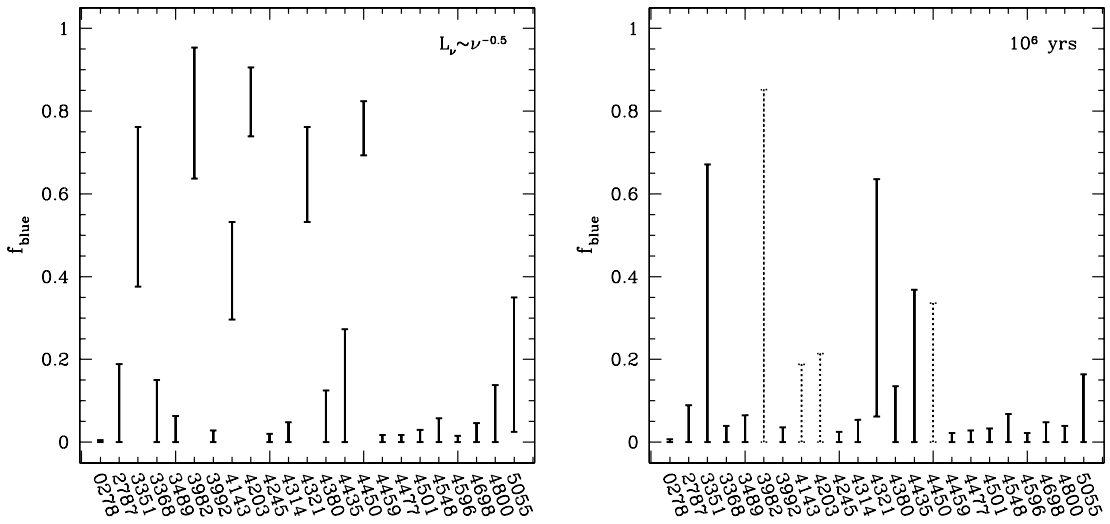

Fig. 8.— Confidence limits (3σ) for the flux fraction in the range 3050–3200 Å from a power-law featureless continuum (for $L_\nu \propto \nu^{-0.5}$, *left panel*), or a single, 10^6-yr-old, starburst population model (*right panel*). The dotted lines identify cases where the need for young stars is most likely overestimated by the models of §4.2. Each number is the NGC name of the galaxy.

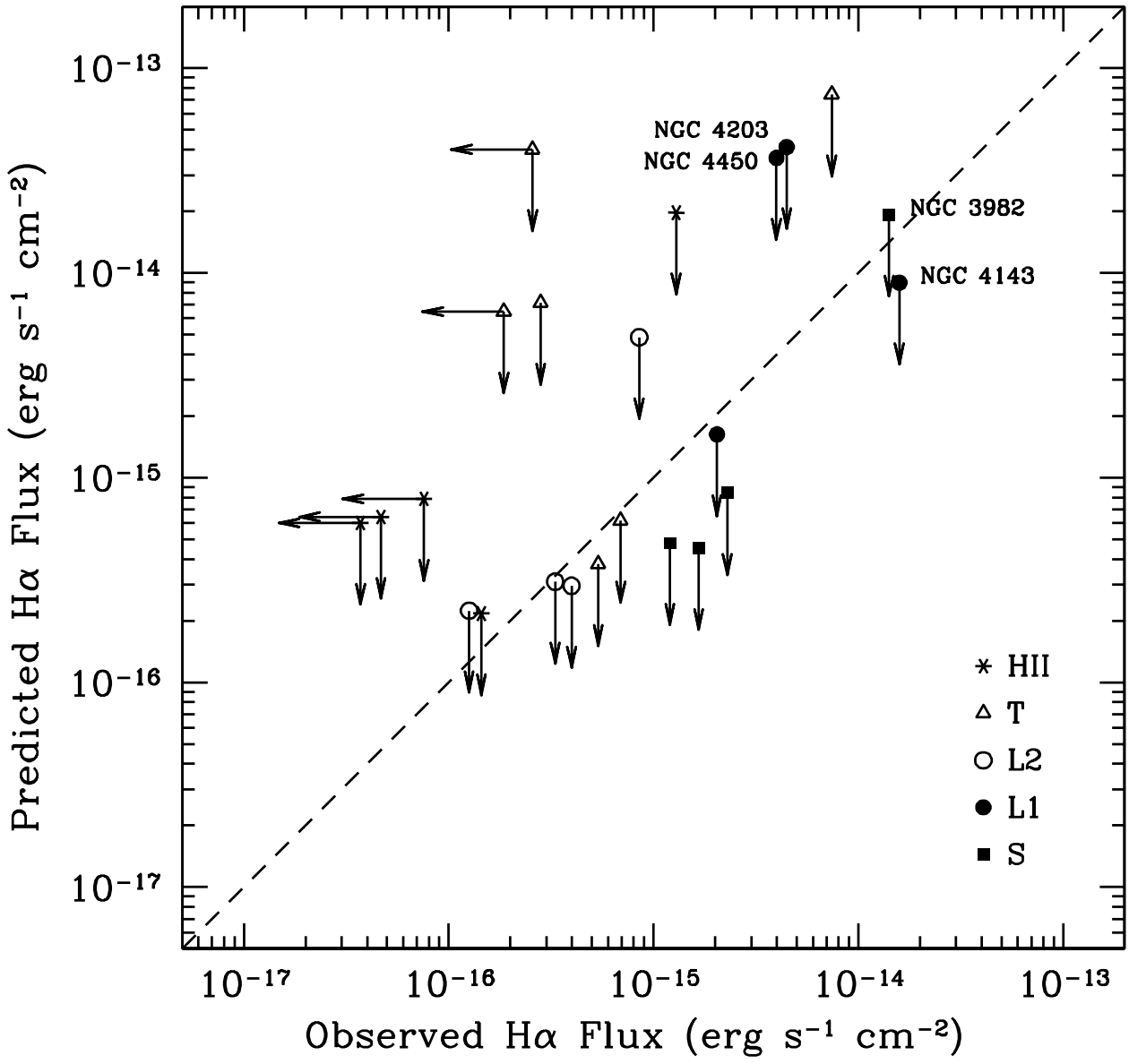

Fig. 9.— Comparison of the predicted Hα fluxes for H II regions powered by the maximum number of young stars indicated by our G430L spectra, and the observed Hα emission in our G750M spectra. The symbol type denotes the ground-based, nuclear emission-line classification of our objects, while the *dashed line* shows the unity, consistency limit. Sources in which the stellar fluxes are probably overestimated due to contamination by an AGN continuum are labeled (NGC 3982, NGC 4143, NGC 4203, and NGC 4450). Correction of the observed Hα emission for internal extinction inferred from the observed decrement of the Balmer emission lines will further shift most plotted points to the right.

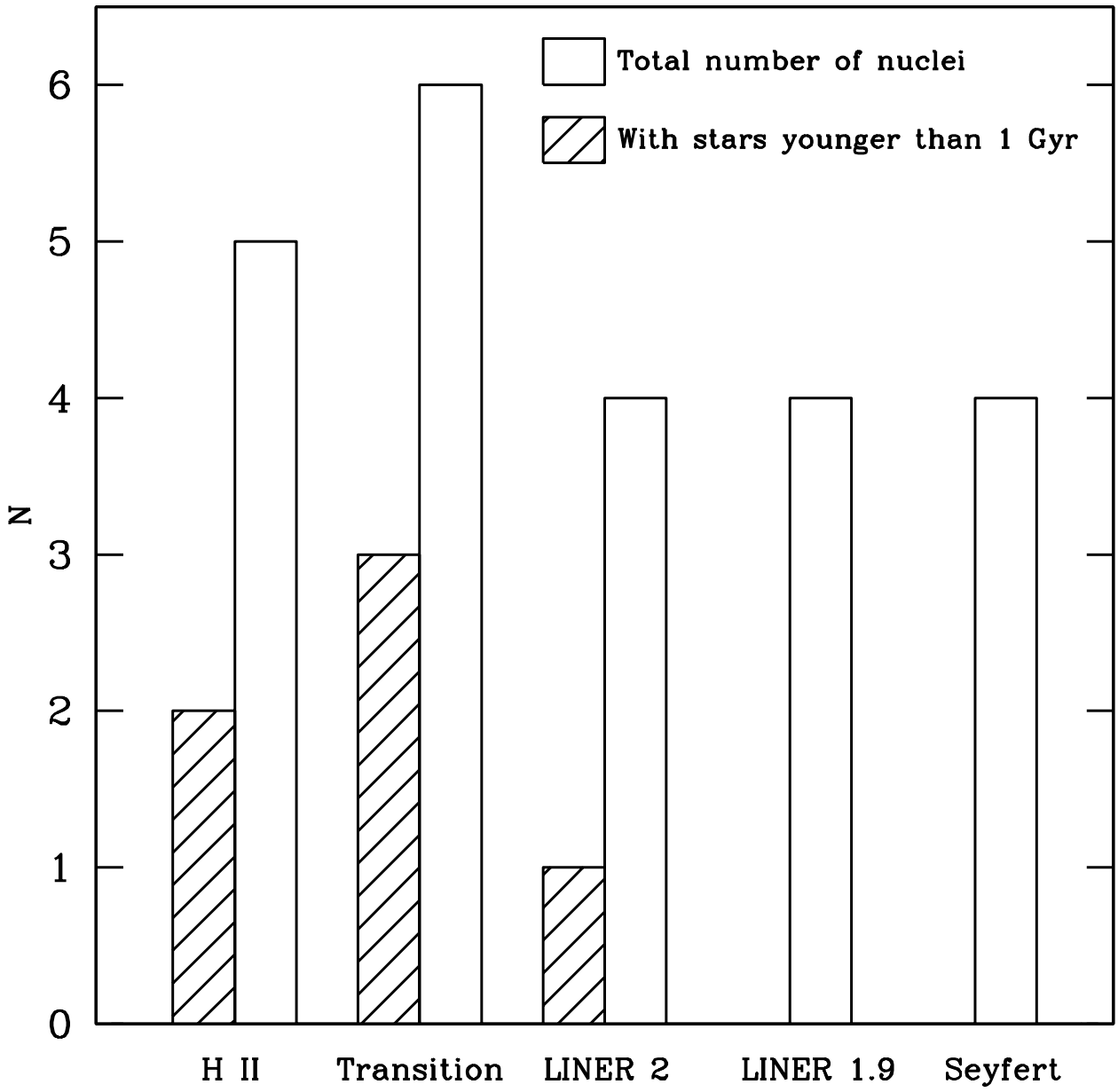

Fig. 10.— Incidence of stars younger that 1 Gyr in the surveyed galactic nuclei as a function of their ground-based spectral classification.

Table 1. Basic Parameters of the Sample Galaxies

Galaxy	Hubble Type	B_T (mag)	Spectral Class	D (Mpc)	i (deg.)	$A_{V,Gal}$ (mag)	$\sigma_\star$ (km s^{-1})	Ref.	Obs. Date
(1)	(2)	(3)	(4)	(5)	(6)	(7)	(8)	(9)	(10)
NGC 278	SABb	11.47	H	11.8	—	0.46	—	—	10 Dec. 1998
NGC 2787	SB0$^+$	11.82	L1.9	13.0	51	0.43	202 ± 5	1	05 Dec. 1998
NGC 3351	SBb	10.53	H	8.1	48	0.09	101 ± 16	2	25 Dec. 1998
NGC 3368	SABab	10.11	L2	8.1	47	0.08	135 ± 10	3	31 Oct. 1998
NGC 3489	SAB0$^+$	11.12	T2/S2	6.4	56	0.05	112 ± 3	1	23 Jan. 1999
NGC 3982	SABb:	—	S1.9	17.0	30	0.05	73 ± 4	1	11 Apr. 1998
NGC 3992	SBbc	10.60	T2:	17.0	53	0.09	140 ± 20	4	19 Feb. 1999
NGC 4143	SAB0°	11.65	L1.9	17.0	52	0.04	270 ± 12	5	20 Mar. 1999
NGC 4203	SAB0$^-$:	11.80	L1.9	9.7	21	0.04	87 ± 3	6	18 Apr. 1999
NGC 4245	SB0/a	12.31	H	9.7	41	0.07	—	—	18 Apr. 1999
NGC 4314	Sba	11.43	L2	9.7	27	0.08	117 ± 4	1	20 Apr. 1999
NGC 4321	SABbc	10.05	T2	16.8	32	0.08	92 ± 4	1	23 Apr. 1999
NGC 4380	SAb:?	12.66	H	16.8	58	0.08	65 ± 19	3	25 Dec. 1999
NGC 4435	SB0°	11.74	T2/H:	16.8	44	0.09	156 ± 7	7	29 Apr. 1999
NGC 4450	Sab	10.90	L1.9	16.8	43	0.09	130 ± 17	2	31 Jan. 1999
NGC 4459	S0$^+$	11.32	T2:	16.8	41	0.15	189 ± 21	1	23 Apr. 1999
NGC 4477	SB0:?	11.38	S2	16.8	24	0.10	156 ± 12	8	23 Apr. 1999
NGC 4501	Sb	10.36	S2	16.8	59	0.12	151 ± 17	9	26 Apr. 1999
NGC 4548	SBb	10.96	L2	16.8	38	0.12	82 ± 9	10	26 Apr. 1999
NGC 4596	SB0$^+$	11.35	L2::	16.8	43	0.07	154 ± 5	11	20 Dec. 1998
NGC 4698	Sab	11.46	S2	16.8	53	0.08	134 ± 6	10	24 Nov. 1997
NGC 4800	Sb	12.30	H	15.2	43	0.05	112 ± 2	1	03 Mar. 1999
NGC 5055	Sbc	9.31	T2	7.2	56	0.06	118 ± 4	1	22 Mar. 1999

Note. — Col. (1): Galaxy name. Col. (2): Hubble type from de Vaucouleurs et al. (1991). Col. (3): Total apparent B magnitude from de Vaucouleurs et al. (1991). Col. (4): Nuclear spectral class from Ho et al. (1997), where H = H II nucleus, L = LINER, S = Seyfert, T = "transition object" (LINER/H II), 1 = type 1, 2 = type 2, and a fractional number between 1 and 2 denotes intermediate type; uncertain and highly uncertain classifications are followed by a single and double colon, respectively. Col. (5): Distance, from Tully (1988), who assumes $H_0 = 75$ km s^{-1} Mpc^{-1}. Col. (6): Galaxy inclination, from Ho et al. (1997). Col. (7): Galactic foreground dust extinction, from Schlegel, Finkbeiner, & Davis (1998). Col. (8): Ground-based central stellar velocity dispersion $\sigma_\star$. Col. (9): Reference for $\sigma_\star$. Col. (10): UT observation date.

References. — (1) Barth et al. 2002, red side; (2) Whitmore, Schechter, & Kirshner 1979; (3) Héraudeau et al. 1999; (4) Sarzi et al. 2002; (5) Di Nella et al. 1995; (6) Dalle Ore et al., 1991; (7) Simien & Prugniel 1997; (8) Jarvis et al. 1988; (9) Héraudeau & Simien 1998; (10) Corsini et al. 1999; (11) Kent 1990.

Table 2. Best Single-Starburst Models

Galaxy	T_{best} log(yr)	A_V (mag)	χ^2_ν
(1)	(2)	(3)	(4)
NGC 278	8.50	0.4	1.85
NGC 2787	10.0	0.0	2.53
NGC 3351	9.25	0.0	1.34
NGC 3368	9.00	0.5	1.88
NGC 3489	9.00	0.3	3.14
NGC 3982	9.25	0.0	2.49
NGC 3992	10.0	0.8	1.52
NGC 4143	9.50	0.1	3.50
NGC 4203	9.25	0.0	17.58
NGC 4245	10.0	0.0	1.43
NGC 4314	10.0	0.3	1.29
NGC 4321	9.00	0.0	7.99
NGC 4380	10.0	0.5	0.72
NGC 4435	9.75	0.4	1.32
NGC 4450	9.25	0.1	8.46
NGC 4459	10.0	0.5	3.63
NGC 4477	10.0	0.6	1.76
NGC 4501	10.0	1.0	1.80
NGC 4548	10.0	0.6	1.20
NGC 4596	10.0	0.2	1.50
NGC 4698	10.0	0.2	1.60
NGC 4800	10.0	0.1	1.56
NGC 5055	9.50	0.0	11.08

Note. — Col. (1): Galaxy name. Col. (2)–(4): Age in Gyr of the best-fitting Bruzual & Charlot (2003) SSP model, required amount of internal extinction, and fit χ^2 divided by the number of degrees of freedom, respectively.

Table 3. Multiple-Starburst Models

Galaxy	$\overline{T}_{light}$ log(yr)	A_V (mag)	χ^2_ν	$L_{\leq 1Gyr}$ %	$M_{\leq 1Gyr}$ %
(1)	(2)	(3)	(4)	(5)	(6)
NGC 278	8.50	0.4	1.86	100.00	100.00
NGC 2787	10.0	0.0	2.56	—	—
NGC 3351	9.39	0.4	0.79	45.16	1.31
NGC 3368	9.51	0.5	1.24	22.66	1.37
NGC 3489	9.49	0.0	1.98	8.95	0.94
NGC 3982	9.29	0.3	1.46	38.70	0.42
NGC 3992	10.0	0.8	1.53	—	—
NGC 4143	9.91	0.2	2.34	19.02	0.15
NGC 4203	9.68	0.5	4.39	45.24	0.32
NGC 4245	9.99	0.0	1.42	1.64	0.06
NGC 4314	10.0	0.3	1.29	—	—
NGC 4321	9.01	0.5	1.58	51.44	2.44
NGC 4380	10.0	0.4	0.72	—	—
NGC 4435	9.95	0.4	1.23	11.98	0.18
NGC 4450	9.79	0.4	2.33	37.82	0.26
NGC 4459	10.0	0.5	3.61	—	—
NGC 4477	10.0	0.6	1.77	—	—
NGC 4501	10.0	1.0	1.81	—	—
NGC 4548	10.0	0.6	1.20	—	—
NGC 4596	10.0	0.2	1.50	—	—
NGC 4698	10.0	0.3	1.60	—	—
NGC 4800	9.99	0.1	1.45	2.10	0.07
NGC 5055	9.87	0.1	10.45	18.43	0.33

Note. — Col. (1): Galaxy name. Col. (2)–(4): Luminosity-weighted mean age corresponding to the optimal combination of templates listed in Table 4, required amount of internal extinction, and fit χ^2 divided by the number of degrees of freedom, respectively. Col. (5)–(6): Cumulative light and mass fraction from single-age B&C models younger than 1 Gyr, respectively. Only the stellar mass of the models is considered; mass lost by stars during their evolution is excluded.

Table 4. Multiple-Starburst Models

Galaxy	$l_{10^{6.0}}$	$l_{10^{6.5}}$	$l_{10^{7.0}}$	$l_{10^{7.5}}$	$l_{10^{8.0}}$	$l_{10^{8.5}}$	$l_{10^{9.0}}$	$l_{10^{9.25}}$	$l_{10^{9.5}}$	$l_{10^{9.75}}$	$l_{10^{10.0}}$
(1)	(2)	(3)	(4)	(5)	(6)	(7)	(8)	(9)	(10)	(11)	(12)
NGC 278	—	—	—	—	—	1.000	—	—	—	—	—
NGC 2787	—	—	—	—	—	—	—	—	—	—	1.000
NGC 3351	—	—	0.253	—	0.199	—	—	—	0.450	—	0.098
NGC 3368	—	—	—	—	0.170	0.057	0.507	—	—	—	0.266
NGC 3489	—	—	—	—	0.006	0.084	0.614	—	—	0.121	0.175
NGC 3982	—	—	0.387	—	—	—	—	—	0.613	—	—
NGC 3992	—	—	—	—	—	—	—	—	—	—	1.000
NGC 4143	—	0.010	—	0.181	—	—	—	—	—	—	0.810
NGC 4203	—	0.252	—	0.200	—	—	—	—	0.104	—	0.444
NGC 4245	—	—	—	—	—	0.016	—	—	—	—	0.984
NGC 4314	—	—	—	—	—	—	—	—	—	—	1.000
NGC 4321	—	—	0.380	—	0.134	—	—	0.376	0.110	—	—
NGC 4380	—	—	—	—	—	—	—	—	—	—	1.000
NGC 4435	0.007	—	—	—	0.113	—	—	—	—	—	0.880
NGC 4450	—	0.155	—	0.223	—	—	—	—	—	—	0.622
NGC 4459	—	—	—	—	—	—	—	—	—	—	1.000
NGC 4477	—	—	—	—	—	—	—	—	—	—	1.000
NGC 4501	—	—	—	—	—	—	—	—	—	—	1.000
NGC 4548	—	—	—	—	—	—	—	—	—	—	1.000
NGC 4596	—	—	—	—	—	—	—	—	—	—	1.000
NGC 4698	—	—	—	—	—	—	—	—	—	—	1.000
NGC 4800	—	—	—	—	—	0.021	—	—	—	—	0.979
NGC 5055	—	—	0.016	—	0.168	—	—	—	0.106	—	0.710

Note. — Col. (1): Galaxy name. Col. (2)–(11): relative light weights of each Bruzual & Charlot (2003) SSP model in the best-fitting multiple starburst model for each nuclear spectrum.

Table 5. Multiple-Starburst Models with $Z = 2.5Z_{\odot}$

Galaxy	$\overline{T}_{light}$ log(yr)	A_V (mag)	χ^2_ν	$L_{\leq 1Gyr}$ %	$M_{\leq 1Gyr}$ %
(1)	(2)	(3)	(4)	(5)	(6)
NGC 278	8.50	0.2	1.50	100.00	100.00
NGC 2787	9.92	0.0	2.29	11.25	0.23
NGC 3351	9.31	0.5	0.79	39.05	0.53
NGC 3368	9.23	0.5	1.22	30.29	2.78
NGC 3489	9.17	0.0	1.76	19.35	3.27
NGC 3982	9.30	0.3	1.45	35.95	0.07
NGC 3992	10.0	0.3	1.07	—	—
NGC 4143	9.85	0.0	2.19	18.81	0.08
NGC 4203	9.58	0.4	4.12	41.99	0.04
NGC 4245	9.89	0.0	1.34	10.80	0.38
NGC 4314	9.97	0.0	1.15	6.52	0.19
NGC 4321	9.10	0.5	1.56	47.36	0.98
NGC 4380	10.0	0.0	0.68	—	—
NGC 4435	9.80	0.3	1.24	15.79	0.20
NGC 4450	9.65	0.3	2.33	32.84	0.03
NGC 4459	10.0	0.0	2.33	0.39	0.01
NGC 4477	10.0	0.1	1.35	—	—
NGC 4501	10.0	0.5	1.40	—	—
NGC 4548	10.0	0.1	1.04	—	—
NGC 4596	9.96	0.0	1.15	8.03	0.24
NGC 4698	9.95	0.0	1.39	2.23	0.07
NGC 4800	9.90	0.0	1.39	7.45	0.26
NGC 5055	9.71	0.1	10.30	13.62	0.14

Note. — Col. (1): Galaxy name. Col. (2)-(6): Luminosity-weighted mean age corresponding to the optimal combination of templates with super-solar metallicities, along with the corresponding required amount of internal extinction, fit χ^2 divided by the number of degrees of freedom, and cumulative light and mass fraction from templates younger than 1 Gyr, respectively.

Table 6. Maximum Predicted Hα Powered by Young Stars

Galaxy	Predicted Hα Flux erg s^{-1}cm^{-2}	Observed Hα Flux erg s^{-1}cm^{-2}
(1)	(2)	(3)
NGC 278	7.9×10^{-16}	$\leq 7.6 \times 10^{-17}$
NGC 2787	1.6×10^{-15}	2.0×10^{-15}
NGC 3351	2.0×10^{-14}	1.3×10^{-15}
NGC 3368	4.8×10^{-15}	8.5×10^{-16}
NGC 3489	6.5×10^{-15}	$\leq 1.9 \times 10^{-16}$
NGC 3982	(1.9×10^{-14})	1.4×10^{-14}
NGC 3992	3.8×10^{-16}	5.4×10^{-16}
NGC 4143	(9.0×10^{-15})	1.5×10^{-14}
NGC 4203	(4.1×10^{-14})	4.5×10^{-15}
NGC 4245	2.2×10^{-16}	1.4×10^{-16}
NGC 4314	3.1×10^{-16}	3.3×10^{-16}
NGC 4321	7.4×10^{-14}	7.4×10^{-15}
NGC 4380	6.0×10^{-16}	$\leq 3.7 \times 10^{-17}$
NGC 4435	7.1×10^{-15}	2.8×10^{-16}
NGC 4450	(3.6×10^{-14})	4.0×10^{-15}
NGC 4459	6.2×10^{-16}	6.9×10^{-16}
NGC 4477	4.8×10^{-16}	1.2×10^{-15}
NGC 4501	8.4×10^{-16}	2.0×10^{-15}
NGC 4548	3.0×10^{-16}	4.0×10^{-16}
NGC 4596	2.2×10^{-16}	1.4×10^{-16}
NGC 4698	4.5×10^{-16}	1.7×10^{-15}
NGC 4800	6.4×10^{-16}	$\leq 4.7 \times 10^{-17}$
NGC 5055	4.0×10^{-14}	$\leq 2.6 \times 10^{-16}$

Note. — Col. (1): Galaxy name. Col. (2): Predicted Hα fluxes from the rate of ionizing photons that would be emitted by the 3σ upper limit on 1-Myr-old stars obtained from our spectra. Predictions that are questionable due to probable power-law contamination of the continuum are indicated in parentheses. Col (3): Observed Hα emission in our G750M spectra (Shields et al. 2004). Upper limits correspond to cases where no clear emission is detected.